# MEASUREMENT OF TRANSITION METALS IN SODA-LIME-SILICATE GLASSES BY USING ELECTRON SPIN RESONANCE (ESR) SPECTROSCOPY

**A Thesis Submitted to**
**the Graduate School of Engineering and Sciences of**
**İzmir Institute of Technology**
**in Partial Fulfillment of the Requirements for the Degree of**

**MASTER OF SCIENCE**

**in Material Science and Engineering**

**by**
**Hakan GÖKTÜRK**

**July 2017**
**İZMİR**

We approve the thesis of **Hakan GÖKTÜRK**

**Examining Committee Members:**

**Asst. Prof. Dr. Yaşar AKDOĞAN**
Department of Materials Science and Engineering, İzmir Institute of Technology

**Asst. Prof. Dr. Ümit Hakan YILDIZ**
Department of Materials Science and Engineering, İzmir Institute of Technology

**Asst. Prof. Dr. Osman AKIN**
Department of Mechatronics Engineering, İzmir Katip Çelebi University

**6 July 2017**

**Asst. Prof. Dr. Yaşar AKDOĞAN**
Supervisor, Department of Materials Science and Engineering,
İzmir Institute of Technology

**Asst. Prof. Dr. Umut ADEM**
Co-Supervisor, Department of Materials Science and Engineering,
İzmir Institute of Technology

**Prof. Dr. Mustafa Muammer DEMİR**
Head of the Department of Materials Science and Engineering

**Prof. Dr. Aysun SOFUOĞLU**
Dean of the Graduate School of Engineering and Sciences

# ACKNOWLEDGEMENTS

There are a lot of people who have assisted me during my graduate education. First of all, I would like to thank Asst. Prof. Dr. Ufuk ŞENTÜRK and Assoc. Prof. Dr. Yaşar AKDOĞAN for their patience, encouragement and excellent guidance on the research which I performed. It was a pleasure for me to work in the field of glass and ESR spectroscopy, and it was honor to study with them.

I would like to special thank Asst. Prof. Dr. Ümit Hakan YILDIZ and Asst. Prof. Dr. Osman AKIN for participating as a committee member and reviewing my work.

I would like to thank my friends Ayser KAYCI, Anıl ÖZDEMİR, Yaman GÖKSEL and Çağatay SARITEPE.

Also I would like to thank Arca İYİEL and ŞişeCam for their supports.

Endless gratitude is also extended to my parents, Barış GÖKTÜRK and Nesrin GÖKTÜRK, my brother Kaan GÖKTÜRK and all my friends for providing love and support every time that I got desperate. I love them very much.

# ABSTRACT


## MEASUREMENT OF TRANSITION METALS IN SODA-LIME-SILICATE GLASSES BY USING ELECTRON SPIN RESONANCE (ESR) SPECTROSCOPY

Electron spin resonance (ESR) spectroscopy does not appear to have found a wide use when compared with other structural analysis methods, especially spectroscopy techniques, utilized in the glass industry. The method, however, provides a good means for supporting the structural information obtained from other spectroscopic methods. Because of its ability to detect and differentiate the paramagnetic ions at low concentrations, ESR spectroscopy is commonly used as a quantitative and qualitative analysis method for evaluating transition metals.

This study showed the behavior and interaction of paramagnetic 3d transition metal ions using ESR spectroscopy for the soda-lime-silicate based glasses. For this reason, it revealed the existence of paramagnetic ($Fe^{3+}$, $Cr^{3+}$, $Mn^{2+}$ and $Cu^{2+}$) transition metal ions in soda-lime-silicate glass and their spectral trends studied at addition levels up to 2.0% mol. Additionally, ESR spectra of $Fe^{3+}$-$Cr^{3+}$, $Fe^{3+}$-$Mn^{2+}$ and $Fe^{3+}$-$Cu^{2+}$ added soda-lime-silicate glass samples were studied to show the effects of the different transition metals on $Fe^{3+}$ containing glasses. The final point of study is that the approach to quantify the ESR spectra with the concentration of paramagnetic metal ions in glass. In this way, this study gives structural information about the used glass and so lightens the locations of used metal ions.

# ÖZET

## SODA KİREÇ SİLİKA CAMLARDA GEÇİŞ METALLERİNİN ELEKTRON SPİN REZONANS (ESR) SPEKTROSKOPİSİ KULLANILARAK ÖLÇÜLMESİ

Elektron spin rezonans (ESR) spektroskopisi, cam endüstrisinde kullanılan diğer spektroskopik yapısal analiz metotları ile kıyaslandığında geniş alan bulamamıştır. Fakat bu metot diğer spektroskopik tekniklerden elde edilen yapısal bilgileri desteklemede iyi bir araçtır. Paramanyetik iyonları düşük konsantrasyonlarda bile saptayabilmesi ve araştırabilmesi sayesinde ESR spektroskopisi geçiş metallerini değerlendirmede kantitatif ve kalitatif analiz metodu olarak yaygınca kullanılmaktadır.

Bu çalışma ESR spektroskopisinin paramanyetik 3d geçiş metal iyonlarının davranış ve etkileşimlerini soda kireç silika camlar için göstermiştir. Bu sebeple, soda kireç silika camların içinde paramanyetik ($Fe^{+3}$, $Cr^{+3}$, $Mn^{+2}$ ve $Cu^{+2}$) geçiş metal iyonlarının molce %2.0'ın altında katkılandığındaki spektral yönelimleri ortaya çıkartılmıştır. Buna ek olarak, farklı geçiş metallerinin $Fe^{+3}$ içeren cam örneklere olan tesirlerini ve etkileşimlerini göstermek için $Fe^{+3}$-$Cr^{+3}$, $Fe^{+3}$-$Mn^{+2}$ ve $Fe^{+3}$-$Cu^{+2}$ eklenmiş soda kireç silika cam örneklerinin ESR spektrumları çalışılmıştır. Çalışmanın son noktası da, cam içerisindeki paramanyetik geçiş metali iyonlarının ESR spektrumlarına olan kantitatif yaklaşımdır. Bu sayede, çalışma kullanılan camın yapısal bilgisi hakkında bilgi vermiştir ve metal iyonlarının cam içerisindeki lokasyonlarını aydınlatmıştır.

# TABLE OF CONTENTS

# LIST OF FIGURES

**Figure** **Page**

# LIST OF TABLES

**Table** **Page**

# LIST OF ABBREVIATIONS

| | |
|---|---|
| ESR | Electron Spin Resonance |
| XPS | X-ray Photoelectron Spectroscopy |
| ZFS | Zero field splitting |

# CHAPTER 1

# INTRODUCTION

## 1.1. General Overview of Glass

Glass is an inorganic amorphous non-crystalline solid [1]. Figure 1.1 shows an illustration of a typical atomic structure arrangement of an $A_2O_3$ type oxide material ion as its amorphous and crystalline form. The figure illustrates the random arrangement of the atomic network when compared with its crystalline counterpart.

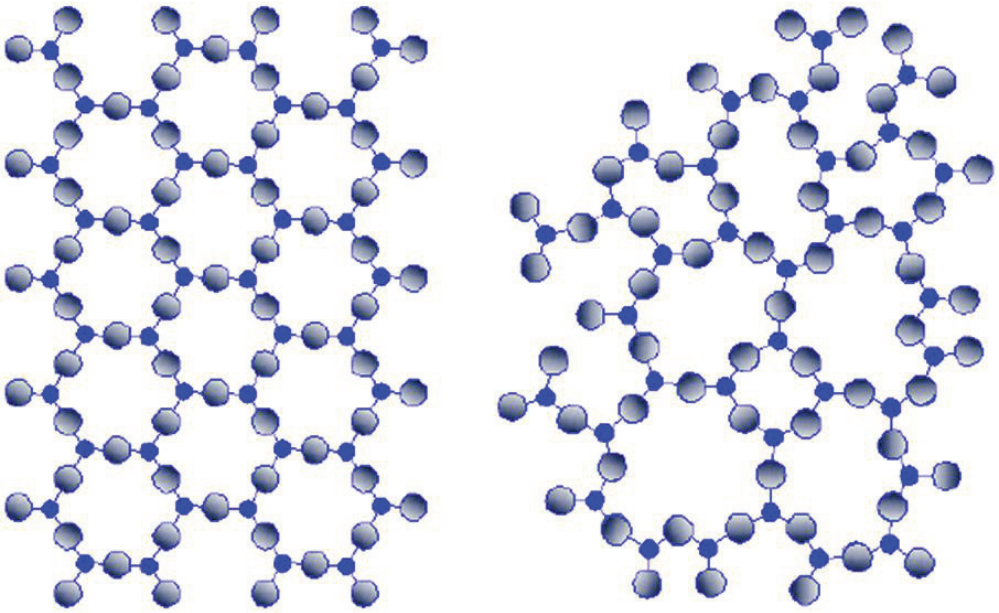

(a) (b)

Figure 1.1. Atomic structure of 2D $A_2O_3$ (a) crystal form (b) glass form[2]

Glass, from its structural standpoint, has three kind of components; network formers, intermediates and network modifiers. Cations that form strong ionic bonds with oxygens also provide the basis for the network structure and are referred to as “Network

Formers". They are p block elements, which means their valence electrons are in p-orbitals. Examples of such oxide network formers are silicon oxide ($SiO_2$), boron trioxide ($B_2O_3$), phosphorus pentaoxide ($P_2O_5$) and germanium dioxide ($GeO_2$). "Intermediates" (such as $Al_2O_3$, PbO) add special characteristic properties to glass. They cannot form glass network by themselves. However, they can replace with network formers or they can join into an existing network. "Network modifiers" cations form slightly weak ionic bonds with oxygens. They are s group elements. They are alkali oxides such as $Na_2O$ and CaO. Their task is to modify glass network for example decreasing the melting temperature of glass [3].

The optical properties of glasses can be examined in three categories:

1. Bulk optical properties such as refractive index and optical dispersion. Bulk optical properties of glass can change or affect diffraction of light which is core principle of telescope or microscope etc. It is argued that bulk properties support to shape development of modern astronomy, biology, and medical science's future.
2. Optical properties that depend on the wavelength, which directly affect color of glass. This color effect can result from ligand field, colloidal metal, etc. Geometric arrangement of transition or rare earth metals, which is related with ligand field theory can change absorption wavelength of glass. Some transition metal ions can combine into atoms by heating process in glass. These atoms affect absorption wavelength of glass. The alteration of absorption wavelength of glass directly affects color.
3. Non-traditional optical effects such as photosensitivity, photochromism, light scattering, etc. Structural properties of photosensitive and photochromic glasses are changed when they are exposed to ultraviolet light, which change the optical properties of glass. Opal glasses are opaque due to light scattering which results from liquid-liquid or liquid-solid phase separation.

These three categories are generated and/or modified by adding transition metals or rare earth metals into the glass structure. Each transition metals or rare earth metals and their different ions result in different colors of the glass (Table 1.1).

Table 1.1. Colors Generated by Transition-Metal and Rare-Earth Ions in Glass [1].

| **Transition Metal Ions** | | | **Rare Earth Ions** | | |
|---|---|---|---|---|---|
| **Configuration** | **Ion** | **Color** | **Configuration** | **Ion** | **Color** |
| $d^0$ | $Ti^{4+}$ | Colorless | $4f^0$ | $La^{3+}$ | None |
| | $V^{5+}$ | Faint yellow to colorless | | $Ce^{4+}$ | Weak yellow |
| | $Cr^{6+}$ | Faint yellow to colorless | $4f^1$ | $Ce^{3+}$ | Weak yellow |
| $d^1$ | $Ti^{3+}$ | Violet-purple | $4f^2$ | $Pr^{3+}$ | Green |
| | $V^{4+}$ | Blue | $4f^3$ | $Nd^{3+}$ | Violet-pink |
| | $Mn^{6+}$ | Colorless | $4f^4$ | $Pm^{3+}$ | None |
| $d^2$ | $V^{3+}$ | Yellow-green | $4f^5$ | $Sm^{3+}$ | None |
| $d^3$ | $Cr^{3+}$ | Green | $4f^6$ | $Sm^{2+}$ | Green |
| $d^4$ | $Cr^{2+}$ | Faint blue | | $Eu^{3+}$ | None |
| | $Mn^{3+}$ | Purple | $4f^7$ | $Eu^{2+}$ | Brown |
| $d^5$ | $Mn^{2+}$ | Light yellow | | $Gd^{3+}$ | None |
| | $Fe^{3+}$ | Faint yellow | $4f^8$ | $Tb^{3+}$ | None |
| $d^6$ | $Fe^{2+}$ | Blue-green | $4f^9$ | $Dy^{3+}$ | None |
| | $Co^{3+}$ | Faint yellow | $4f^{10}$ | $Dy^{2+}$ | Brown |
| $d^7$ | $Co^{2+}$ | Blue-pink | | $Ho^{3+}$ | Yellow |
| $d^8$ | $Ni^{2+}$ | Brown-purple | $4f^{11}$ | $Er^{3+}$ | Weak pink |

**(Cont. on next page)**

Table 1.1. (Cont.)

| | | | | | |
|---|---|---|---|---|---|
| $d^9$ | $Cu^{2+}$ | Blue-green | $4f^{12}$ | $Tm^{3+}$ | None |
| $d^{10}$ | $Cu^{+}$ | Colorless | $4f^{13}$ | $Tm^{2+}$ | None |
| | | | | $Yb^{3+}$ | None |
| | | | $4f^{14}$ | $Lu^{3+}$ | None |

## 1.2. Electron Spin Resonance (ESR) Spectroscopy

Electron paramagnetic resonance (EPR) or electron spin resonance (ESR) spectroscopy determines and measures paramagnetic materials with at least one unpaired electron [4].

ESR spectrometer measures the energy differences between the electron spin states at the resonance condition. Applied external magnetic field separates the energy levels of spin states until the energy difference is equal to the energy of the microwave source. At this point the unpaired electron changes its spin state by absorbing the microwave radiation [4]. This absorption signal is converted into the ESR spectrum after taking its first derivative. Figure 1.2 shows the common representation of an ESR spectrum.

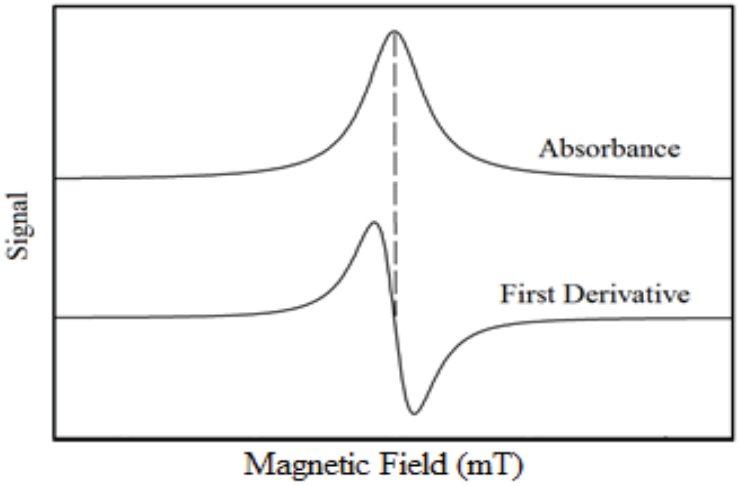


Figure 1.2. Representation of absorbance and first derivative modes of an ESR spectrum.

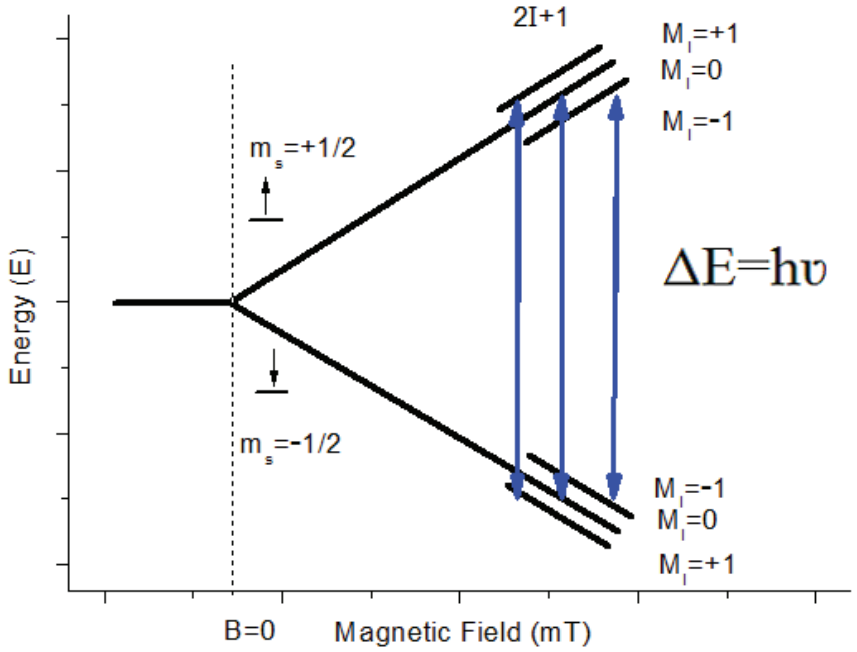


Figure 1.3. Splitting of energy levels of an unpaired electron spin.

Electron has a magnetic moment and a spin quantum number. For every single electron, s refers spin quantum number (s=1/2) and $m_s$ refers spin magnetic moment component ($m_s$= ±1/2). Under magnetic field ($B_o$), spin magnetic moment component of electron is divided into parallel ($m_s$= -1/2) and antiparallel ($m_s$= +1/2) to external field as shown in Figure 1.3. Each of them has individual different energy due to the Zeeman effect:

$$E=m_s g_e \beta B_o \qquad (1.1.)$$

$g_e$ is g factor ($g_e$=2.0023 for free electron), β is Bohr magneton (β=9.2700949 x $10^{-24}$ $JT^{-1}$) and $B_o$ is external magnetic field. Consequently, the difference between magnetic components ($m_s$= ±1/2 and $m_s$= -1/2) is:

$$\Delta E= g_e \beta B_o \text{ for an unpaired electron} \qquad (1.2.)$$

This equation shows that energy levels are proportional to external magnetic field as shown in Figure 1.3. The difference between energy levels is equal to microwave photon energy (ΔE=hυ where h=Planck's constant, υ=microwave frequency), which results in principle equation of ESR spectroscopy [5]:

$$\Delta E= h\upsilon = g_e \beta B_o \qquad (1.3.)$$

An unpaired electron can be affected by applied external magnetic field ($B_o$) and also by local magnetic field ($B_{local}$) paramagnetic species, ligand fields, magnetic nuclei etc. Both of them can contribute to effective magnetic field ($B_{eff}$):

$$B_{eff} = B_o + B_{local} \quad (1.4.)$$

$B_{local}$ can be induced by applied field, which means that value of $B_{local}$ depends on applied magnetic field ($B_o$) [6]. Hence, it can be written:

$$B_{eff} = B_o(1-\sigma) \quad (1.5.)$$

$\sigma$ is the effect of local field. Hence, ESR equation changes at resonance condition:

$$\Delta E = h\upsilon = g_e\beta B_{eff} \rightarrow \Delta E = h\upsilon = g_e\beta B_o(1-\sigma) \quad (1.6.)$$

$g_e(1-\sigma)$ is expressed as g which is called g-factor. The final ESR equation becomes:

$$\Delta E = h\upsilon = g\beta B_o \quad (1.7.)$$

The unpaired electron or the magnetic field of unpaired electron is affected by nearby nuclear spin ($I \neq 0$). This results in additional splitting which is called "Hyperfine Coupling" [7]. Splitting number is expressed as:

$$\text{Splitting number} = 2nI+1 \quad (1.8.)$$

n is number of effective nuclei nearby unpaired electron, I is the nuclear spin number which is taken from Table 1.2. It shows spin number and abundance of some atoms and their isotopes.

Table 1.2. Natural abundance and nuclear spin number of some atoms and their isotopes. (Source: IUPAC, 1998).

| **Atom** | **Isotope** | **Spin(abundance)** |
|---|---|---|
| H | 1, 2 | $^{1}$H 1/2 (99.985), $^{2}$H 1 (0.015) |
| N | 14, 15 | $^{14}$N 1 (99.632), $^{15}$N 1/2 (0.368) |
| O | 16, 17, 18 | $^{17}$O 5/2 (0.038) |
| Mn | 55 | 5/2 (100.000) |
| Fe | 54, 56, 57, 58 | $^{57}$Fe 1/2 (2.119) |
| Cu | 63, 65 | $^{63}$Cu 3/2 (69.17), $^{65}$Cu 3/2 (30.83) |
| Cr | 50, 52, 53, 54 | $^{53}$Cr 3/2 (9.501) |

For instance, MnO (I=5/2) has 6 hyperfine splittings as shown in Figure 1.4. The nuclear spin number of Mn is 5/2 and the number of effective nuclei nearby unpaired electron of $^{55}$Mn is 1. Nuclear spin number of oxygen (ligand of Mn) is zero. Hence:

$$\text{number of splitting} = (2.(1).(5/2))+1= 6 \qquad (1.9.)$$

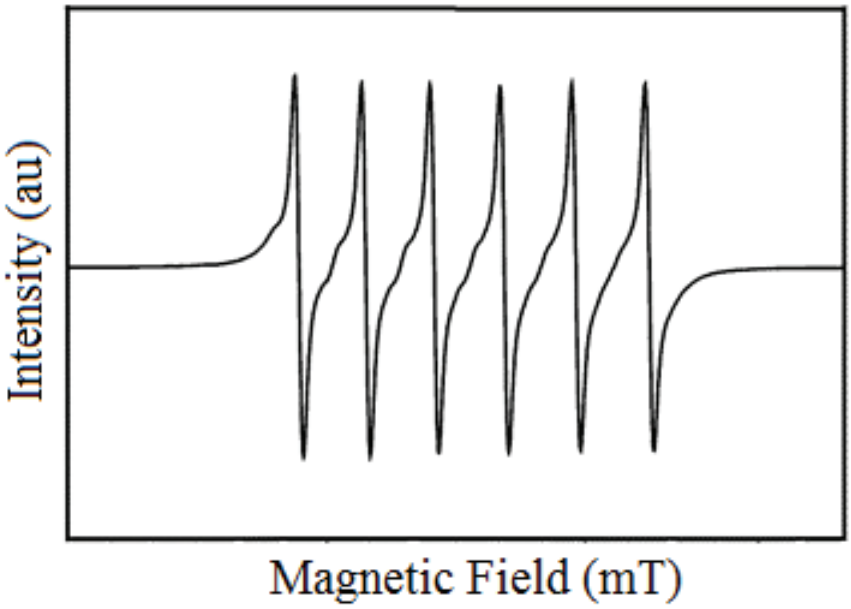


Figure 1.4. ESR spectrum of MnO [8].

CuO (I=3/2) has 4 hyperfine splittings marked as blue lines in Figure 1.5. The nuclear spin number of Cu is 3/2 and the number of effective nuclei nearby unpaired electron of Cu is 1. Nuclear spin number of oxygen (ligand of Cu) is zero. Hence:

$$\text{number of splitting} = (2.(1).(3/2))+1= 4 \qquad (1.10.)$$

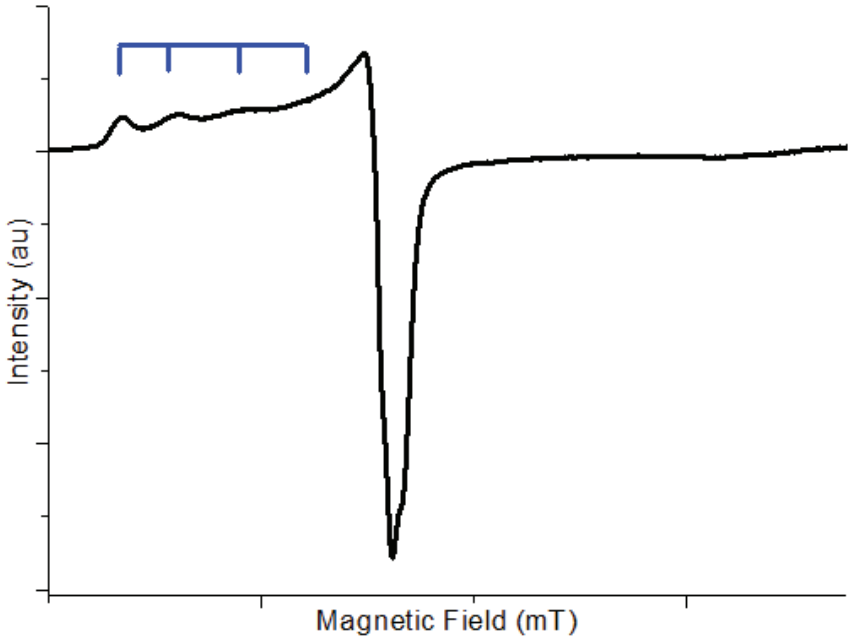


Figure 1.5. ESR spectrum of CuO in soda-lime-silicate glass.

In quantum mechanics, if there are several different energy states with the same energy level, it is called degeneracy of energy states [9]. Degeneracy of energy states is reduced under magnetic field. However, zero field splitting (ZFS) occurs even in the absence of an external magnetic field. ZFS is described as disappearance of spin microstate degeneracy even in the absence of magnetic field [10]. Alteration or distortion of crystal field symmetry causes deviation. These deviations refer ZFS parameters (D and E). D and E refer axial and transversal components of magnetic interaction, respectively [11]. The ZFS parameters are stated by second order terms in the spin Hamiltonian. Hamiltonian is the operator in quantum mechanics. It represents total energy (kinetic and potential) of a system. The total energy corresponds to Hamiltonian operator and it is represented by H or $\hat{H}$. Each system has individual particle or particles. Each particle has different kinetic energy and potential energy. The sum of kinetic energies and potential energies are represented by Hamiltonian. Hamiltonian operator (H or $\hat{H}$) can show alteration depending on type of system and number of particle such as one particle, free particle, electric dipole in an electric field, magnetic dipole in a magnetic field. ESR spectroscopy deals with magnetic dipole in a magnetic field [12]. In this condition, spin Hamiltonian is used. As mentioned earlier, ZFS parameters (D and E) are stated by second order terms in the spin Hamiltonian:

$$H = g\beta B_o S + D\,[S_z^{\,2} - (1/3)\,S(S+1)] + E\,[S_x^{\,2} - S_y^{\,2}] \qquad (1.11.)$$

β is the Bohr magneton, $B_o$ is the magnetic field vector, S is the electron spin operator. $S_x$, $S_y$ and $S_z$ are the spin matrices which means that g tensor consists of $g_x$, $g_y$ and $g_z$ values (principal g-factors). These three g values depend on principal axis system of molcule. In powder samples, ESR spectrum can show differences depending on symmetry of same paramagnetic ion because alteration of the symmetry cause alteration of $g_x$, $g_y$ and $g_z$ values. If the symmetry of paramagnetic ion is isotropic shape (e.g. octahedron, tetrahedron), it gives isotropic spectrum with $g_x=g_y=g_z$. If the symmetry of paramagnetic ion is axially symmetric or symmetry of paramagnetic ion is distorted to axially symmetry, it gives one of two different spectra with $g_x=g_y>g_z$ and $g_x=g_y<g_z$. If the symmetry of paramagnetic ion has rhombic symmetry or symmetry of paramagnetic ion is distorted to rhombic symmetry, it gives one spectrum with $g_x\neq g_y\neq g_z$ as shown in Figure 1.6. However, these conditions are valid for ideal circumstances. Increasing temperature, increasing concentration of paramagnetic ions, changing difference between $g_x$, $g_y$ and $g_z$ values or changing population of different symmetries of the same paramagnetic ions can cause a change of ESR spectrum.

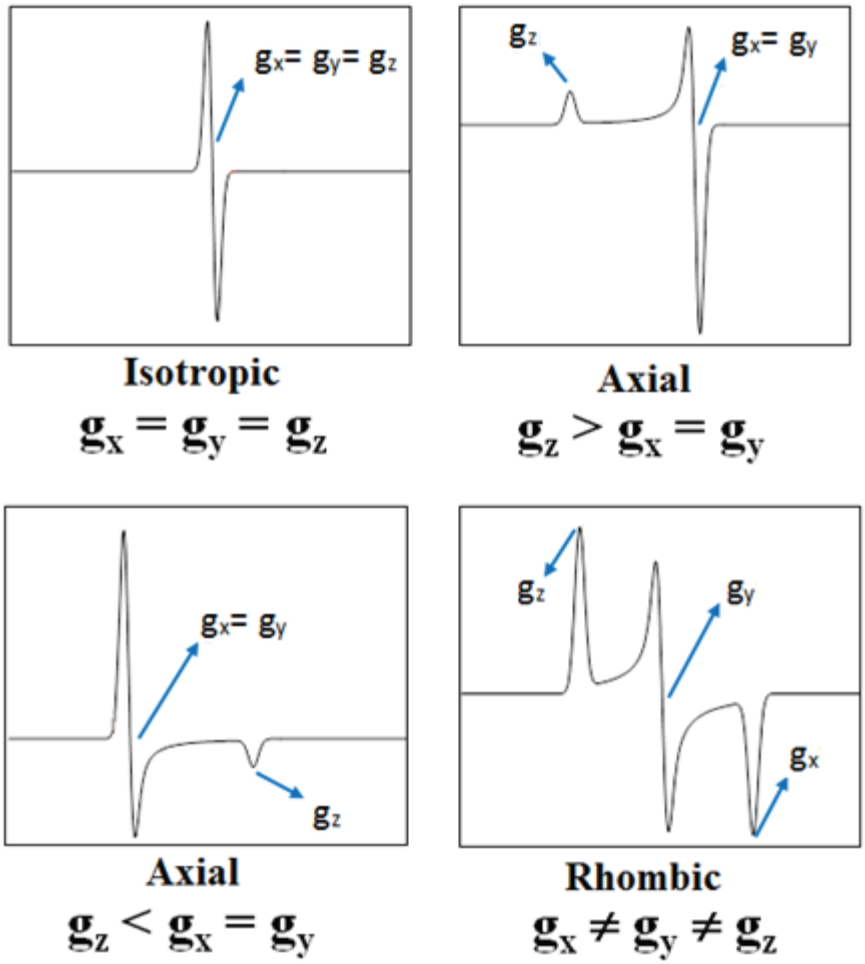


Figure 1.6. ESR spectra of powder samples depending on principal g-factors [13].

When crystal field symmetry of $Fe^{3+}$ ion ($d^5$) is cubic, ZFS parameters equal to zero (D=0 and E=0). In this circumstance, spin quantum numbers ($m_s$) corresponding to energy states degenerate in the absence of magnetic field. This degeneracy is lifted under external magnetic field and energy levels split equally. In this way, five ESR transitions ($m_s$ = ±5/2, ±3/2, ±1/2) are allowed with $\Delta m_s$= ±1 at the same resonant value due to isotropy shown in Figure 1.7 a [14]. These allowed ESR transitions give signal at g≈2 in ESR the spectrum. When octahedral or tetrahedral symmetry of $Fe^{3+}$ is distorted to axial or rhombic symmetry, ZFS parameters are D ≠ 0, E = 0 and D > E ≠ 0, respectively. In this circumstance, energy state degeneracy is reduced even in the absence of external magnetic field and this gives 3 Kramer's doublets ($m_s$ = ±5/2, ±3/2, ±1/2) as shown in Figure 1.7 b. If splitting between Kramer's doublet is high (compare to microwave energy) which means large rotation of symmetry to axial or rhombic, the only one ESR transition is allowed between $m_s$ = -1/2 and $m_s$ = +1/2. The other four transition are not

allowed due to high anisotropy. When rhombic distortion is maximum, ESR transition gives two signals which are single line at g ≈ 4.2 and also weak and broad line at g ≈ 9.0 in ESR spectrum. When axial distortion is maximum, ESR transition gives one signal at g ≈ 6.0 [15].

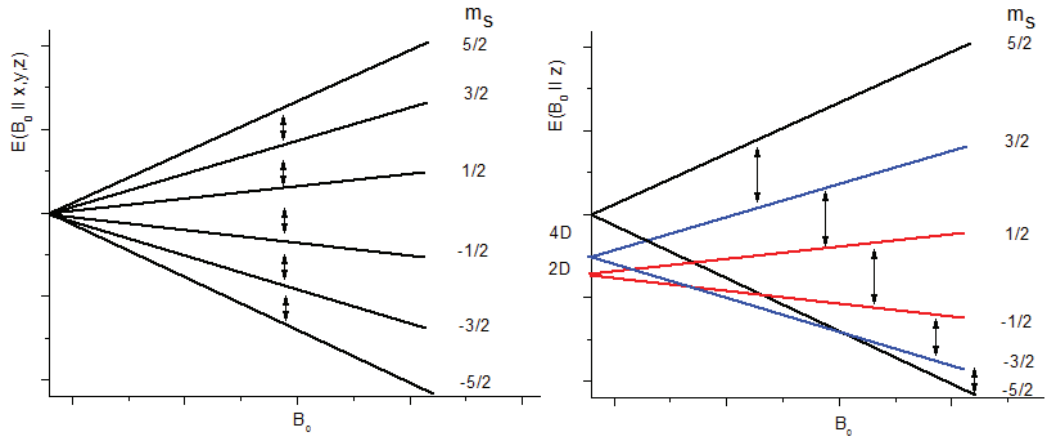


Figure 1.7. Schematic representation of energy level splitting for isolated $Fe^{3+}$ ions in high symmetry (a) and axial distortion (b) [14].

## 1.3. Literature Survey on ESR Spectroscopy of Glasses

Iron plays an important role in the field of glass research and technology since iron is present as an impurity in the raw materials of glass. Iron ions enter into the glass chemistry and its structure either as an unwanted or an uncontrolled impurity element or as a purposefully formulated dopant.

Ruangthaweep *et al.* [16] studied the addition of iron into a soda-lime silicate glass composition, where the formulation has been given as (65-x) $SiO_2$: 25$Na_2O$: 10CaO: x$Fe_2O_3$. This glass composition was studied at $Fe_2O_3$ concentrations from 0.00 to 0.50 mol percentages. They showed the paramagnetic $Fe^{3+}$ ions in the ESR spectra and explained the signals behaviors at g=4.3 and g=2.1. They showed that the signal at g=4.3 is associated with rhombic distortion of octahedral or tetrahedral symmetry of $Fe^{3+}$ ions and signal at g=2.1 is associated with $Fe^{3+}$ ions located as cluster in glass. They concluded that the $Fe^{3+}$ signal increases by increasing the amount of $Fe_2O_3$. This behavior is related to the changes in the color of glass. Rüssel [17] showed the effects of iron addition on lithium, sodium, potassium and cesium containing lime and silicate based glass

compositions. Rüssel [18], in another study showed the effects of sodium ions on a potassium containing mixed alkali lime silicate glasses. All of these studies concluded that amount and types of alkali metals affect location (in cluster or in glass network) of the transition metal ions. Transition metals interact with non-bridging oxygens in glass where transition metals locate as cluster or they attend to glass network by forming Si-O-(Transition metal)-O-Si bond. This alkali metal effect is caused by changing number of non-bridging oxygens and also stability of transition metal ions in glass.

Nattapon *et al*. [19] showed effect of paramagnetic manganese ion content on soda-lime-silicate glass. The signal near g=4.3 has been linked to the distortion of octahedral symmetry of $Mn^{2+}$ to rhombic symmetry. At g=2.0, octahedral symmetry of $Mn^{2+}$ in clusters is distorted and sextet lines appear which arises from interaction between electron spin and nuclear spin in manganese, called hyperfine interaction. These hyperfine splittings disappear with increasing concentration of manganese.

Nobuya *et al*. [20] showed effect of partial oxygen pressure on the oxidation states of chromium ions ($Cr^{3+}$ and $Cr^{5+}$) in soda-lime-silicate glasses. Oxidation states of chromium ions, $Cr^{3+}$ and $Cr^{5+}$ were showed by using ESR spectroscopy. Three signals were observed which depend on amount of chromium content and CO pressure in ESR spectrum. When CO pressure increases, the oxidation state of chromium changes from $Cr^{3+}$ to $Cr^{2+}$ so the ESR signal disappears. At g=4, the signal results from isolated $Cr^{3+}$ ions in an orthorhombic field. Isolated $Cr^{5+}$ ions cause signal at g=2.3. Coupled $Cr^{3+}$ ion pairs are observed at g=2.

Dacapito *et al*. [21] showed effect of alkali ion exchange which is done by $CuSO_4$:$Na_2SO_4$ and $CuSO_4$:$K_2SO_4$ salt bath on state of copper ion in soda-lime-silicate glass. Isolated $Cu^{2+}$ ions replace with alkali species in glass and the signal of $Cu^{2+}$ ions are located at g=2.0 in the ESR spectrum. Dacapito showed that alkali ion exchange affects optical response of soda-lime-silicate glass like refractive index. Refractive index depends on quantity of transition metal content which can be effected by alkali species.

ESR spectroscopy has been also used to investigate paramagnetic metal ions in non-silicate glasses. Kesavulu *et al*. [22] studied the effect of changing lithium content on paramagnetic chromium ions in a lithium-cesium borate type glasses. Lakshmana *et al*. [23] studied the effects of both CuO and $Cr_2O_5$ additions, and the effect of temperature on $KSO_4$-$ZnSO_4$ based sulphate glasses. Kesavulu *et al*. [24] studied effect of paramagnetic chromium ions on borate glasses ($Li_2O$–$Cs_2O$–$B_2O_3$). Lakshmana and Kesavulu showed

the behavior of paramagnetic chromium ions with ESR spectroscopy. At near g=4.0, the signal is associated with isolated $Cr^{3+}$ ions which are in octahedral environments. At near g=2, there are two kinds of signals which are attributed to the $Cr^{3+}$- $Cr^{3+}$ and $Cr^{5+}$- $Cr^{5+}$ interactions. Adam *et al*. [25] showed the effect of changing CuO and $MnO_2$ contents on $CaB_4O_7$ and $LiCaBO_3$ based borate glasses. Prakash *et al*. [26], studied the effects of paramagnetic copper ions content on sodium fluoride-sodium borate glasses, and evaluated the molcular orbital coefficients. Both of these studies showed that the $Cu^{2+}$ ions replaced with alkali species present as isolated ions, and they are found at the octahedral sites in the glass structure. If octahedrally coordinated $Cu^{2+}$ ions elongate parallel to z-axis, it is represented as $g_{\text{II}}$=2.3 while the octahedrally coordinated $Cu^{2+}$ ions that elongate perpendicular to z-axis is represented as $g_{\perp}$=2.0.

## 1.4. Motivation

ESR spectroscopy does not appear to have found a wide use when compared with other structural analysis methods, especially spectroscopy techniques, utilized in the glass industry. The method, however, provides a good means for supporting the structural information obtained from other spectroscopic methods. Because of its ability to detect and differentiate the paramagnetic ions, ESR spectroscopy is commonly used as a quantitative and qualitative analysis method for evaluating transition metals. This is also a valid approach for the techniques application in glasses. The knowledge of the form and amount of transition metal ions in the structure of the material is important since these can affect the properties (e.g: optical, mechanical, etc.) of glass.

In this study, we aim to provide an approach and an understanding on the below listed key areas related to the use of ESR spectroscopy applied to a soda-lime-silica based glass composition with addition of the different transition metal ions.

- Understanding the operation of the ESR spectrometer used in this study as it applies to the analysis of glasses. To do this, we used Fe ions dissolved in a soda-lime silicate glass matrix at different concentrations. Iron is a transition metal that has been widely studied using ESR to date. As such, the findings from this study aims to compare and correlate our experimentation with what is known and adopted in the literature.
- Understanding the ESR spectra of soda-lime silicate glasses those have another transition metal added to their structures in addition to iron in the glass composition.

We have not found a systematic study in this area, hence another aim in this particular area is to provide ESR spectral information on the interactions that may be present in dual transition metals added glass formulations.

- Understanding if ESR spectroscopy can be used to quantitatively characterize the presence of paramagnetic $Fe^{3+}$ ions in soda-lime silicate glasses.
- Understanding the structural nature of the paramagnetic transition metal ions in soda-lime silicate glasses.

# CHAPTER 2

# EXPERIMENTAL STUDY

## 2.1. Materials and Methods

All chemical reagents were either obtained from commercial supplier (Aldrich, Aldrick, Alfa Aesar and Emsure) and Sisecam AS (Table 2.1). All glass samples was produced in electrical furnace which is Protherm PC442. ESR was measured with Adani CMS 8400 ESR spectrometer.

Table 2.1. The alternative names and source of materials

| Material | Alternative Name | Source |
|---|---|---|
| $SiO_2$ | Sand | ŞİŞECAM |
| $CaCO_3$ | Lime | ŞİŞECAM |
| $Na_2CO_3$ | Soda | Aldrich |
| $Fe_2O_3$ | Iron(III) oxide | Aldrich |
| $CrCl_3*6H_2O$ | Chromium(III) chloride hexahydrate | Aldrick-27096-100GF |
| $MnO_2$ | Manganese(IV) oxide | Fluka-63548-1KG-F |
| $Cu_2O$ | Copper(I) oxide | Alfa Aesar-A14436 |
| $CoCl_2*6H_2O$ | Cobalt(II) chloride hexahydrate | Emsure-1.02539 |

## 2.2. Processing of Glass Compositions

Each glass composition was weighed and prepared in mol percentage as shown in Table 2.2. However they were not proved with other spectroscopic methods after production of glass samples.

Table 2.2. Glass Compositions.

| Sample Identification | $SiO_2$ | CaO | $Na_2O$ | $Fe_2O_3$ | $Cr_2O_5$ | $MnO_2$ | CuO | CoO |
|---|---|---|---|---|---|---|---|---|
| **1.Base** | 65 | 10 | 25 | - | - | - | - | - |
| **2.1.Base+Fe** | 65 | 10 | 25 | 0.05 | - | - | - | - |
| **2.2** | 65 | 10 | 25 | 0.1 | - | - | - | - |
| **2.3** | 65 | 10 | 25 | 0.3 | - | - | - | - |
| **2.4** | 65 | 10 | 25 | 0.5 | - | - | - | - |
| **2.5** | 65 | 10 | 25 | 1.0 | - | - | - | - |
| **2.6** | 65 | 10 | 25 | 2.0 | - | - | - | - |
| **3.1.Base+Cr** | 65 | 10 | 25 | - | 0.1 | - | - | - |
| **3.2** | 65 | 10 | 25 | - | 0.3 | - | - | - |
| **3.3** | 65 | 10 | 25 | - | 0.5 | - | - | - |
| **3.4** | 65 | 10 | 25 | - | 1.0 | - | - | - |
| **3.5** | 65 | 10 | 25 | - | 2.0 | - | - | - |
| **4.1.Base+Fe+Cr** | 65 | 10 | 25 | 0.05 | 0.1 | - | - | - |
| **4.2** | 65 | 10 | 25 | 0.05 | 0.3 | - | - | - |
| **4.3** | 65 | 10 | 25 | 0.05 | 0.5 | - | - | - |
| **4.4** | 65 | 10 | 25 | 0.3 | 0.1 | - | - | - |
| **4.5** | 65 | 10 | 25 | 0.3 | 0.3 | - | - | - |
| **4.6** | 65 | 10 | 25 | 0.3 | 0.5 | - | - | - |
| **4.7** | 65 | 10 | 25 | 0.025 | 0.5 | - | - | - |
| **4.8** | 65 | 10 | 25 | 0.05 | 0.5 | - | - | - |
| **4.9** | 65 | 10 | 25 | 0.06 | 0.5 | - | - | - |
| **4.10** | 65 | 10 | 25 | 0.1 | 0.5 | - | - | - |
| **5.1.Base+Cu** | 65 | 10 | 25 | - | - | - | 0.1 | - |

**(Cont. on next page)**

Table 2.2. (Cont.)

| | | | | | | | | |
|---|---|---|---|---|---|---|---|---|
| **5.2** | 65 | 10 | 25 | - | - | - | 0.3 | - |
| **5.3** | 65 | 10 | 25 | - | - | - | 0.5 | - |
| **6.1.Base+Fe+Cu** | 65 | 10 | 25 | 0.05 | - | - | 0.1 | - |
| **6.2** | 65 | 10 | 25 | 0.05 | - | - | 0.3 | - |
| **6.3** | 65 | 10 | 25 | 0.05 | - | - | 0.5 | - |
| **6.4** | 65 | 10 | 25 | 0.3 | - | - | 0.1 | - |
| **6.5** | 65 | 10 | 25 | 0.3 | - | - | 0.3 | - |
| **6.6** | 65 | 10 | 25 | 0.3 | - | - | 0.5 | - |
| **7.1.Base+Mn** | 65 | 10 | 25 | - | - | 0.1 | - | - |
| **7.2** | 65 | 10 | 25 | - | - | 0.3 | - | - |
| **7.3** | 65 | 10 | 25 | - | - | 0.5 | - | - |
| **8.1.Base+Fe+Mn** | 65 | 10 | 25 | 0.05 | - | 0.1 | - | - |
| **8.2** | 65 | 10 | 25 | 0.05 | - | 0.3 | - | - |
| **8.3** | 65 | 10 | 25 | 0.05 | - | 0.5 | - | - |
| **8.4** | 65 | 10 | 25 | 0.3 | - | 0.1 | - | - |
| **8.5** | 65 | 10 | 25 | 0.3 | - | 0.3 | - | - |
| **8.6** | 65 | 10 | 25 | 0.3 | - | 0.5 | - | - |

## 2.2.1. Batch Preparation

A constant composition representing a soda-lime-silicate type glass has been used as a base formulation throughout this study. This composition is 25Na2O-10CaO-65SiO2, where the values in the formulation is given in mol %. Each component was weighed for 120 g batch and then add to a 140 ml refractory aluminum oxide crucible (Nanotech, Eskişehir). Materials in the crucible were mixed with metal spatula. After that, the crucible was put into elevator type electrical furnace. In furnace, temperature increased until 1350oC for 2 hours in order to avoid breaking of crucible because of

thermal shock. Then, temperature stayed constant at 1350oC for 4 hours. After heating process was done, glassy liquid in the crucible was quenched in water. When cooling process was done, glass particles were put into oven to be dried. In oven, glass particles were stayed at 100ºC for few hours. Then, dried glass particles crashed in ceramic mortar and became powder, which was ready for addition of transition metal.

### 2.2.2. Melting and Forming of Glass Compositions

10 gram of base composition which was mentioned at previous section was weighed for each sample and then add to 140 ml refractory aluminum oxide crucible. After that, metals were weighed with respects to Table 2.2 and put into crucibles. In industry, glass samples are ladled over and over again or glassy liquid is mixed during heating process in order to produce homogenously. However, 10 gram of samples were not sufficient amount for this process. That's why, glass particles and metal powder were mixed with metal spatula in crucible. After that, the crucible was put into elevator type electrical furnace. In furnace, temperature increased until 1350ºC for 2 hours in order to avoid breaking of crucible because of thermal shock. Then, temperature stayed constant at 1350ºC for 4 hours. After heating process was done, glassy liquid in the crucible was quenched in water. When cooling process was done, glass particles were put into oven to be dried. In oven, glass particles were stayed at 100ºC for few hours.

## 2.3. ESR Analysis of Glass Compositions

The glass particles which were dried in oven (prepared in previous section 2.2.2) were crashed in ceramic mortar. Powder of glass samples were added to quartz ESR tube with height of 2.3 cm for each sample. Experiments were done at 23-28ºC and constant pressure. The parameters of ESR measurements are listed in Table.2.3.

Table.2.3. Parameters of ESR Measurements.

| | **Fe and Cr** | **Co, Mn and Cu** |
|---|---|---|
| **Center field** | 250 mT | 350 mT |
| **Sweep width** | 400 mT | 600 mT |
| **Mod. Amplitude** | 200 uT | 200 uT |
| **Power attenuation** | 13 dB | 13 and 26 dB |
| **Gain value** | $1*10^2$ | $1*10^2$ |
| **Sweep time** | 100 s | 100 s |
| **Microwave frequency** | 9441-9443 MHz | 9441-9443 MHz |
| **Room Temperature** | 23-28$^oC$ | 23-28$^oC$ |

# CHAPTER 3

# RESULTS AND DISCUSSION

## 3.1 ESR Measurements of Transition Metals in Glass

### 3.1.1 $Fe_2O_3$ Containing Soda-Lime-Silicate Glass

$Fe^{3+}$ ion has $d^5$ orbital and its total spin number is S=5/2. Hence, it splits into three Krames' doublets, ±5/2, ±3/2 and ±1/2. However, -1/2→+1/2 transition is allowed for powder samples and other four transitions is not allowed due to high anisotropy. That's why, $Fe^{3+}$ gives one signal at ESR spectrum. Figure 3.1 shows the ESR spectrum of $Fe_2O_3$ containing soda-lime-silicate glass. The figure shows two significant characteristic g values at g=4.2 and g=2.0. The signal at g=4.2 and weak signal at g=9.6 [27-28] are associated with the rhombic distortion of tetrahedral or octahedral coordination of $C_{2v}$ symmetry of $Fe^{3+}$ which locates in network structure of glass (Si-O-Fe-O-Si) [16]. The signal at g=2.0 is associated with $Fe^{3+}$ ions located as clusters in glass structure and $Fe^{3+}$-$Fe^{3+}$ interaction. [14].

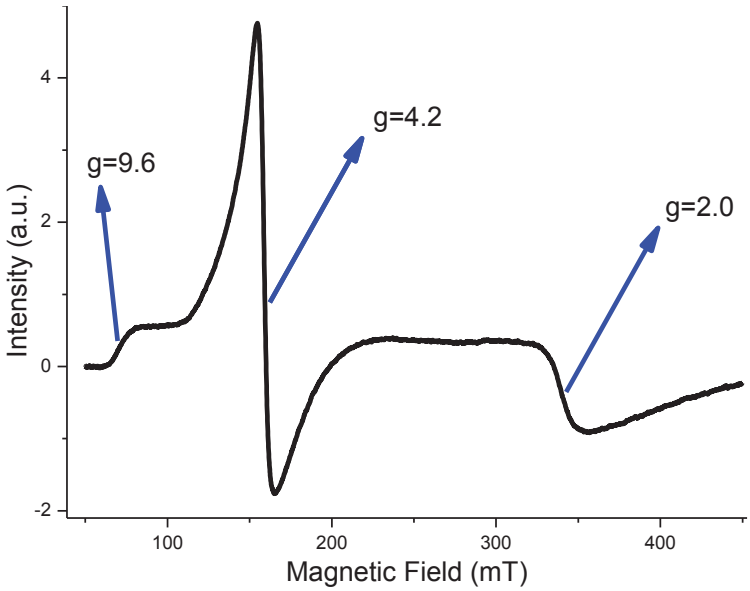


Figure 3.1. ESR spectrum of $Fe_2O_3$ containing soda-lime-silicate glass ($25Na_2O$-$10CaO$ $65SiO_2$-$0.5Fe_2O_3$)

Figure 3.2 shows the ESR spectra of 6 different levels of $Fe_2O_3$ (in a range of 0.05 – 2.00 mol %) containing base compositions ($25Na_2O$-$10CaO$-$65SiO_2$), which were named as 2.1 to 2.6 at Table 2.2. Signal intensities of $Fe^{3+}$ at g=9.6, g=4.2 and g=2.0 increase with increasing amount of $Fe_2O_3$. However, changes in the signal intensities are different at g=2.0 in comparison to g=9.6 and g=4.2.

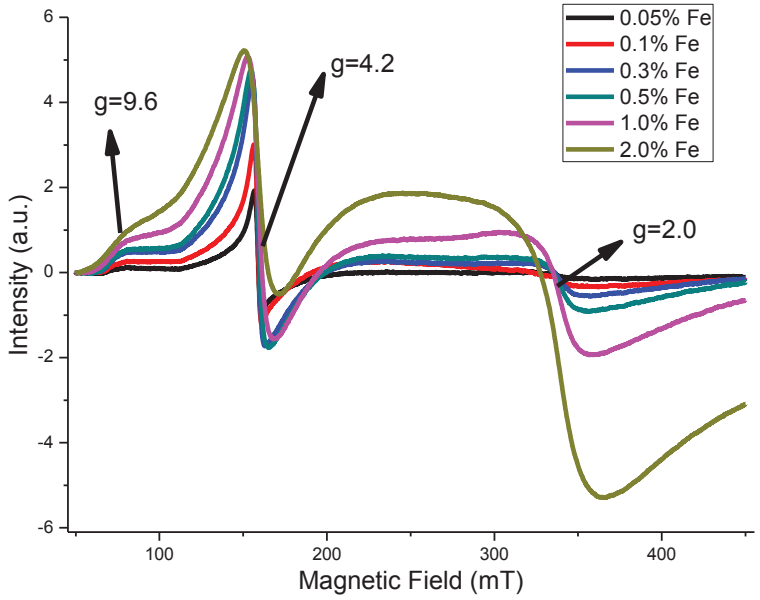


Figure.3.2. ESR spectra of glasses ($25Na_2O$-$10CaO$-$65SiO_2$-$xFe_2O_3$ x=0.05 to 2.0 mol %)

In Figure 3.2, it was also observed that with increasing amount of $Fe_2O_3$ content in glass, signal rises of $Fe^{3+}$ at g=4.2 and g=9.6 are slower compared to the signal at g=2.. The signal intensities at Figure 3.3 were taken from ESR spectra (Figure 3.2). The change in the intensities can be also represented by the area under the spectrum. In order to get quantitative relation between percentage of iron content and area under the spectrum, the area at g=4.2 (x=0 to 270 mT) and the area at g=2 (x=270 to 450 mT) were calculated. Hence, with increasing amount of $Fe_2O_3$ content in glass, the percentage of $Fe^{3+}$ ions that locate in glass network decreases and the percentage of $Fe^{3+}$ ions that locate as cluster in glass increases as shown also in Figure 3.4. It is assumed that with increasing amount of $Fe_2O_3$ content, the number of $Fe^{3+}$ ions locate in glass network reaches saturation level and thus most of the $Fe^{3+}$ ions locate as cluster in glass structure.

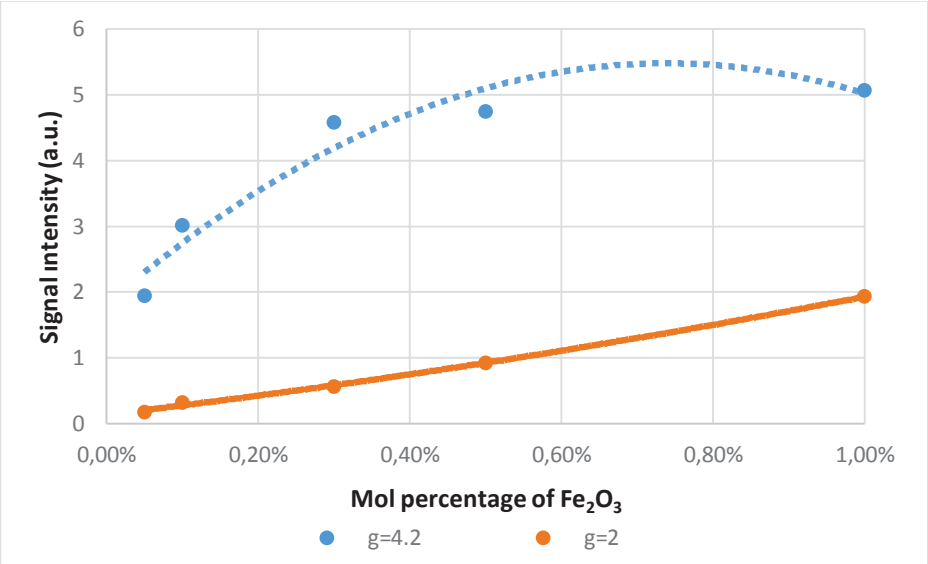


Figure 3.3. Signal intensity of $Fe^{3+}$ (from Figure 3.2) at g=4.2 and g=2.0 vs. mol percentages of $Fe_2O_3$

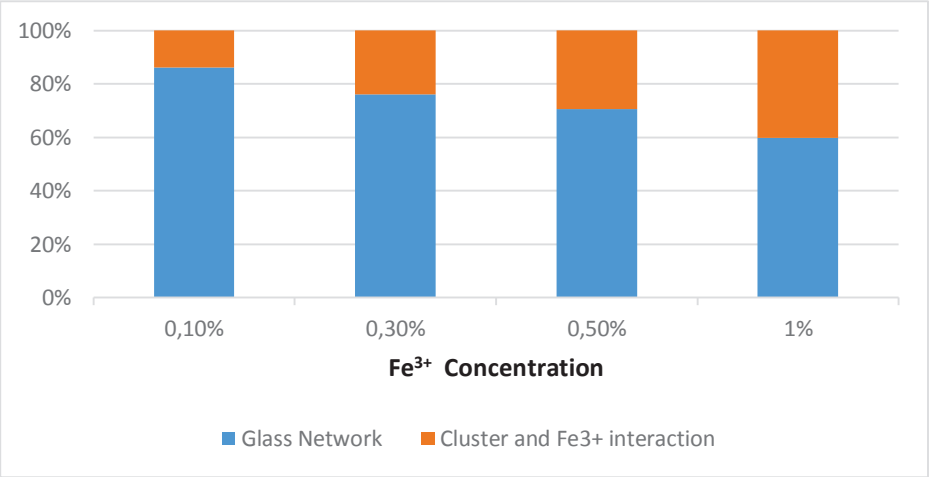


Figure 3.4 Location of $Fe^{+3}$ ions vs. mol percentages of $Fe_2O_3$ in glass

### 3.1.2. $Cr_2O_5$ Containing Soda-Lime-Silicate Glass

Figure 3.5 shows three levels of $Cr_2O_5$ containing soda-lime-silicate glass samples with these compositions; $25Na_2O$-$10CaO$-$65SiO_2$-$xCr_2O_5$ (x=0.1, 0.3, 0.5) after cooling process. They were firstly analyzed in terms of optical properties of glasses. $Cr^{3+}$ ion gives green color to glass and color intensity is directly proportional to $Cr^{3+}$ concentration (from Table 1.1). Figure 3.5 shows that intensity of green color of glass sample increases with increasing amount of $Cr_2O_5$.

Figure 3.5. Crucible samples of [$25Na_2O$-$10CaO$-$65SiO_2$-$yCr_2O_5$ (y=0.1, 0.3 and 0.5 mol %)] after cooling process.

After visual analyze, ESR method was used in order to observe $Cr^{3+}$ species in glass. Figure 3.6 shows the ESR spectrum of $Cr_2O_5$ containing soda-lime-silicate glass sample with composition; $25Na_2O$-$10CaO$-$65SiO_2$-$0.5Cr_2O_5$. $Cr^{3+}$ has $d^3$ orbital and its total spin number is S=3/2. Hence, it splits into two Krames' doublets, ±3/2 and ±1/2. There are three ESR transition is allowed between these Krames' doublets (-3/2→-1/2, -1/2→+1/2, +1/2→+3/2). However, -1/2→+1/2 transition is allowed for powder samples and also other two transitions are not allowed due to high anisotropy. The glass sample includes $Fe_2O_3$ as an impurity (0,003 mol %). Figure 3.6 shows 4 significant characteristic values of g. The signal at g=5.2 is associated with rhombic distortion of octahedral coordination of $Cr^{3+}$ ions in glass network. It is assumed that the signal at g=4.2 is associated with octahedral coordination with $C_{2v}$ symmetry of impurity $Fe^{3+}$. The signal at g=2.1 is associated with $Cr^{3+}$ clusters in glass. The signal at g=2.0 is associated with $Cr^{5+}$ ion ($Cr^{5+}$ ion is also paramagnetic) clusters in glass. $Cr^{5+}$ ion has $d^1$ orbital and its total spin number is S=1/2. $Cr^{5+}$ ion occur probably during glass melting process with partly oxidation of $Cr^{3+}$ ion to $Cr^{5+}$ ion [22, 24].

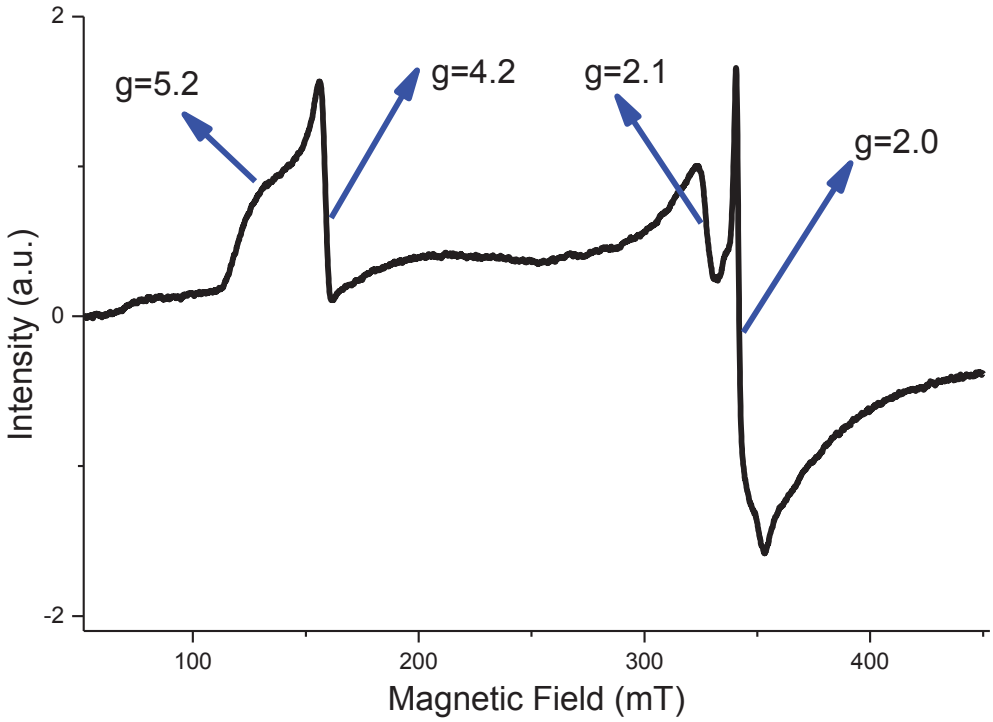


Figure 3.6. ESR spectrum of $Cr_2O_5$ containing soda-lime-silicate glass [$25Na_2O$-10CaO-$65SiO_2$-$0.5Cr_2O_5$].

Figure 3.7 shows the ESR spectra of 3 different levels of $Cr_2O_5$ containing base compositions [$25Na_2O$-10CaO-$65SiO_2$-$xCr_2O_5$(x=0. 1, 0.3, 0.5)], which were named as 3.1 to 3.5 at Table 2.2. Signal intensities at each g values (5.2, 4.2, 2.1 and 2.0) increase with increasing amount of $Cr_2O_5$. However, the signal at g=4.2 could not be explained very well. It is assumed that this signal comes from $Fe^{3+}$ impurity but when the amount of $Cr_2O_5$ increases, the signal intensity at g=4.2 increases as well. It can be concluded that the signals of $Fe^{3+}$ and $Cr^{3+}$ ions overlap around g=5.2 and g=4.2, and the signal of $Fe^{3+}$ does not influence the anisotropy in glass at these levels.

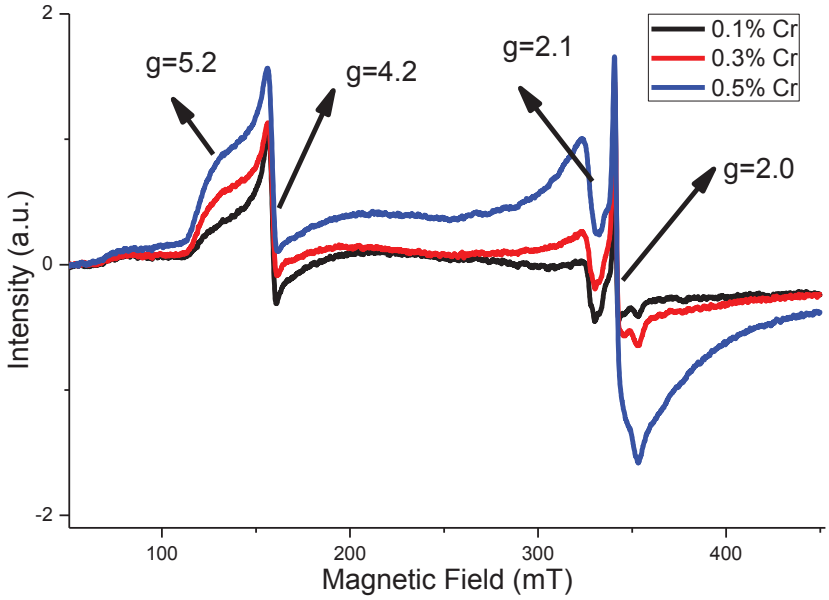


Figure 3.7. ESR spectra of $Cr_2O_5$ containing glasses [$25Na_2O$-$10CaO$-$65SiO_2$-$xCr_2O_5$(x=0. 1, 0.3 and 0.5 mol %)]

The change of signal intensities as a function of $Cr_2O_5$ amount is different in Figure 3.7. The signal intensities at g=5.2 ($Cr^{3+}$ ions located in glass network) and g=2.1 ($Cr^{3+}$ ions located as cluster in glass) are crucial to observe location of $Cr^{3+}$ ions in glass. Figure 3.8 shows that signal intensities of $Cr^{3+}$ ions at g=5.2 and at g=2.1 obtained from Figure 3.7. Figure 3.8 shows that mol percentages ratio of $Cr^{3+}$ ions located in glass network with respect to $Cr^{3+}$ ions located as cluster decreases with increasing amount of $Cr_2O_5$ content (The signal intensity rise of $Cr^{3+}$ ions located in glass network shows a decreasing trend). It is assumed that glass network starts to reach saturation level of $Cr^{3+}$ with increasing amount of $Cr_2O_5$ content and $Cr^{3+}$ ions start to locate as cluster rather than locate in glass network. Kesavulu *et al.* showed that with increasing amount of $Cr_2O_5$ content, the signals around at g=5.2 and g=4.2 start to vanish and the signals around at g=2.0 start to overlap and give one strong isotropic signal. This is because, the signal which is associated with $Cr^{3+}$ ions located as cluster (around g=2.0 or g=2.1) increases too much and overlaps with the other signals. However, this occurs at high level of $Cr_2O_5$ content like 5.0 mol % in glass, which is out of our work range [22, 24].

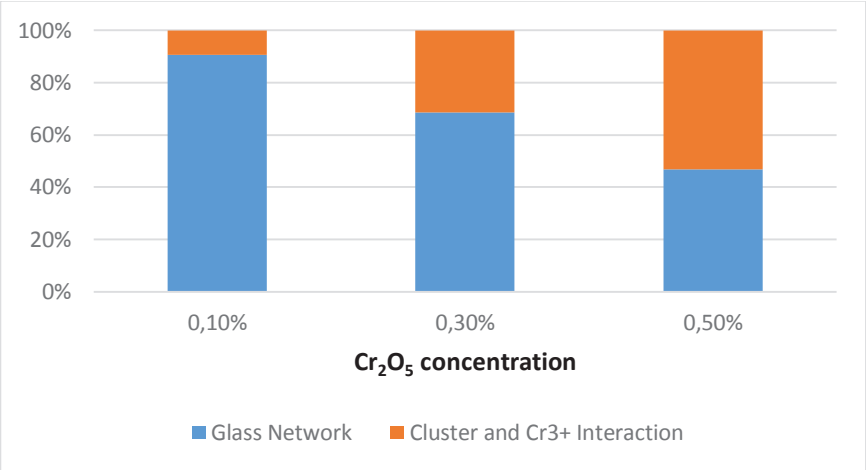


Figure 3.8. Location of $Cr^{+3}$ ions vs. mol percentage of $Cr_2O_5$ in glass

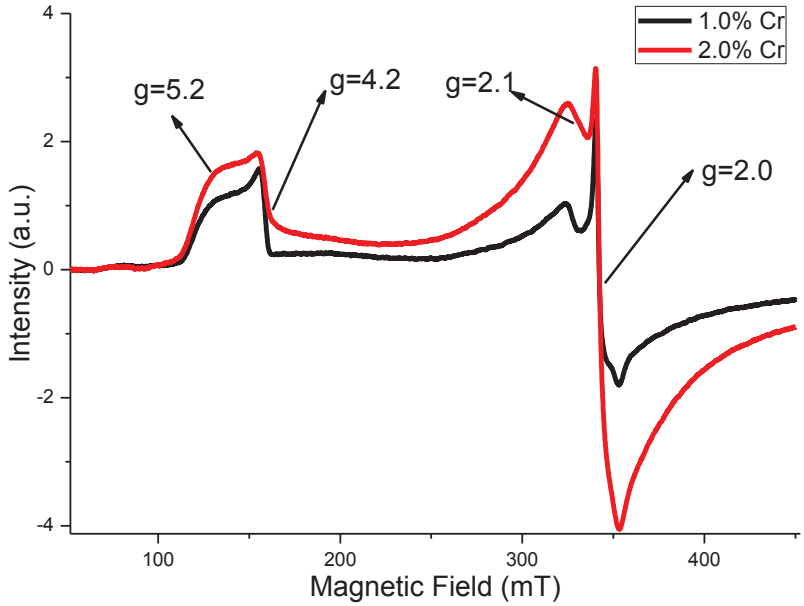


Figure 3.9. ESR spectra of $Cr_2O_5$ containing glass samples [$25Na_2O$-$10CaO$-$65SiO_2$-$xCr_2O_5$(x=1 and 2 mol %)]

Figure 3.9 shows that the signal at g=4.2 start to vanish with amount of 1.0 mol and 2.0 mol % $Cr_2O_5$ or the signal at g=4.2 is overlapped with signal of $Cr^{3+}$. This vanishing shows that the signal at g=4.2 can be associated with $Fe^{3+}$ impurity otherwise it should keep increasing. High addition level of $Cr_2O_5$ may cause anisotropy in glass structure for $Fe^{3+}$ ions. That's why, the signal at g=4.2 may vanish.

To observe interactions between $Fe^{3+}$-$Cr^{3+}$ and $Fe^{3+}$-$Cr^{5+}$ signals in ESR spectroscopy, different glass compositions were prepared. Figure 3.10 shows EPR spectra of glasses that have these compositions; $25Na_2O$-$10CaO$-$65SiO_2$-$0.3Fe_2O_3$-

$xCr_2O_5$(x=0.1, 0.3 and 0.5). Compositions were also named as 4.4 to 4.6 at Table.2.2. Figure 3.10 shows four characteristic g values at g=9.6, g=4.2, g=2.1 and g=2.0. The signal at g=9.6 and g=4.2 is associated with $Fe^{3+}$ ions in glass network. Increasing the $Cr_2O_5$ content decreases the signal of $Fe^{3+}$ ions at g=4.2. This can be explained by the anisotropy increases in the glass structure [25]. The signal at g=2.1 is associated with $Cr^{3+}$ ions located as cluster (or $Cr^{3+}$-$Cr^{3+}$ couples) in the glass structure. The signal at g=2.0 is associated with signal overlapping of $Fe^{3+}$ and $Cr^{5+}$ ions located as cluster. The characteristic signal of $Fe^{3+}$ at g=2.0 can be observed in 0.1% $Cr_2O_5$ containing sample. However, with increasing amount of $Cr_2O_5$ content, the characteristic signal of $Fe^{3+}$ cannot be seen very well and it is overlapped by the signal of $Cr^{5+}$ ions due to high anisotropy. The signal at g=5.2 which is associated with rhombic distortion of octahedral coordination of $Cr^{3+}$ ions in glass network cannot be seen. This is because, the signal of $Fe^{3+}$ ions at g=4.2 may block them (and/or due to anisotropy) [22, 24]. The same situation is valid for the signal of $Cr^{3+}$ and $Cr^{5+}$ ions at g=2.1 and g=2.0, respectively. The characteristic signal of $Cr^{3+}$ and $Cr^{5+}$ ions cannot be seen clearly. It is assumed that addition 0.3 mol % level of $Fe_2O_3$ to glass, may increase randomness of $Cr^{3+}$ and $Cr^{5+}$ ions (it is also known anisotropy) which causes signal loss [25].

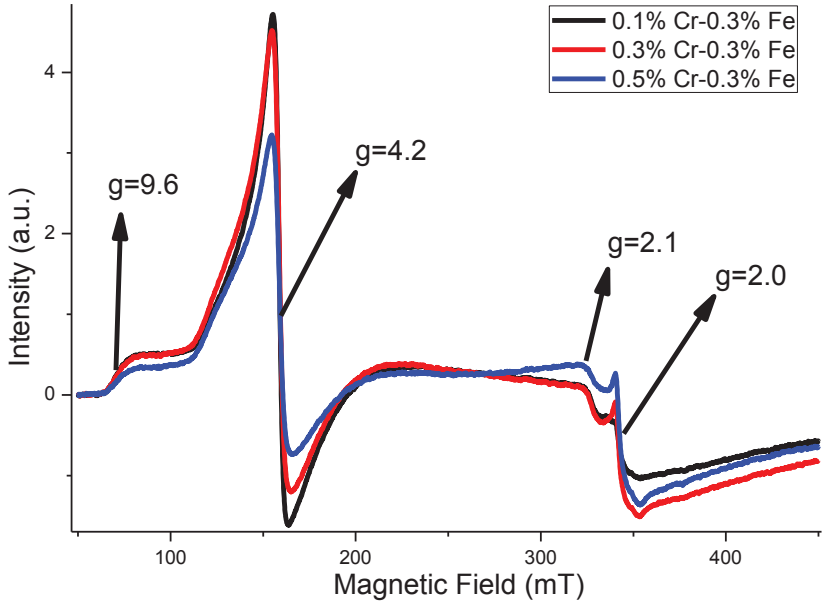


Figure 3.10. ESR spectra of $Fe_2O_3$ and $Cr_2O_5$ containing glass samples [$25Na_2O$-10CaO-$65SiO_2$-$0.3Fe_2O_3$-$xCr_2O_5$(x=0.1, 0.3 and 0.5 mol %)]

Figure 3.11 shows ESR spectra of addition 0.05 mol % $Fe_2O_3$ content to three different levels of $Cr_2O_5$ containing soda-lime-silicate glass samples [$25Na_2O$-10CaO-$65SiO_2$-$0.05Fe_2O_3$-$xCr_2O_5$ (x=0.1, 0.3 and 0.5)] in order to observe signal behavior of $Cr^{3+}$ ions at g=5.2 with addition of $Fe^{3+}$ ions. Signal intensities of $Cr^{3+}$ ions at g=2.1 and $Cr^{5+}$ ions at g=2.0 (in Figure 3.11) decrease in comparison to only $Cr_2O_5$ containing glass samples (in Figure 3.7). It is assumed that rise of $Fe_2O_3$ content in glass causes randomness in glass. Hence, the signal intensities at g=2.1 and g=2.0 decrease due to anisotropy in glass structure [25]. However, signal intensities of $Cr^{3+}$ ions at g=5.2 increase with addition of $Fe_2O_3$ content. This is because, signal of $Fe^{3+}$ ions at g=4.2 overlap with signal of $Cr^{3+}$ ions at g=5.2. This overlapping blocks to observe fall of signal intensities at g=5.2 due to rise of anisotropy (like at g=2.1 and g=2.0).

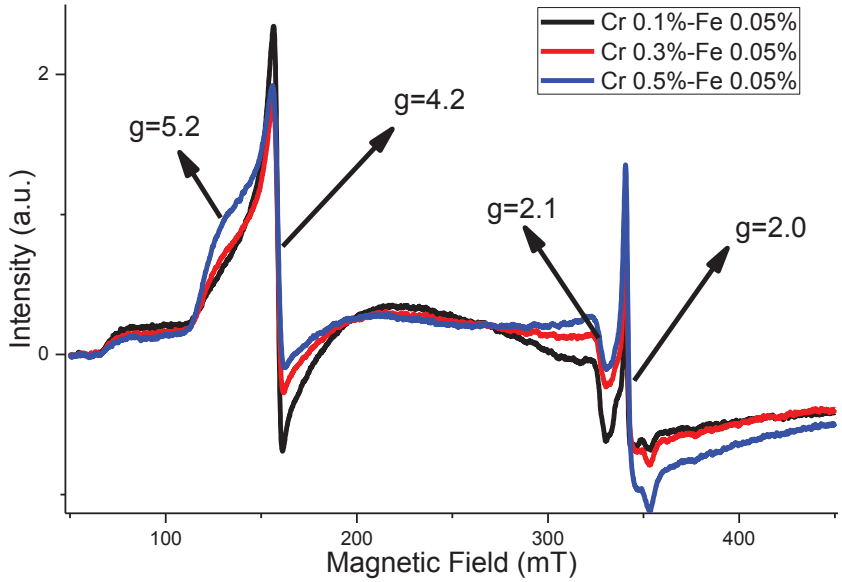


Figure 3.11. ESR spectra of $Fe_2O_3$ and $Cr_2O_5$ containing glass samples [$25Na_2O$-10CaO-$65SiO_2$-$0.05Fe_2O_3$-$xCr_2O_5$(x=0.1, 0.3 and 0.5 mol %)]

Figure 3.12 shows ESR spectra of addition 0.5 mol % $Cr_2O_5$ content to three different levels of $Fe_2O_3$ containing soda-lime-silicate glass samples [$25Na_2O$-10CaO-$65SiO_2$-0.5 $Cr_2O_5$-x $Fe_2O_3$ (x=0.025, 0.06, 0.1)] in order to observe signal behavior of $Cr^{3+}$ ions and $Cr^{5+}$ ions with $Fe^{3+}$ ion at g=2.1 and g=2.0, respectively. The signal intensities of $Cr^{3+}$ ions at g=2.1 (in Figure 3.11) and $Cr^{5+}$ ions at g=2.0 are two times less than in only 0.5 mol % $Cr_2O_5$ containing glass sample (in Figure 3.7). It is assumed that

the rise of $Fe_2O_3$ content in glass causes randomness in glass. Hence, the signal intensities of $Cr^{3+}$ and $Cr^{5+}$ decrease due to anisotropy in glass structure [25].

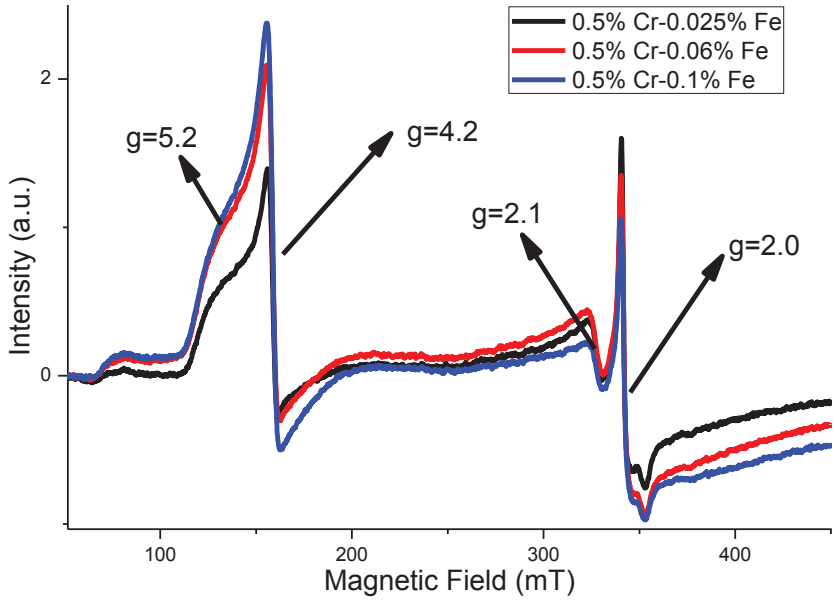


Figure 3.12. ESR spectra of Fe2O3 and Cr2O5 containing glass samples [25Na2O-10CaO-65SiO2-xFe2O3-0.5$Cr_2O_5$(x=0.025, 0.05, 0.06 and 0.1 mol %)].

Figure 3.13 shows signal intensities of $Cr^{3+}$ ions at g=5.2 and g=2.1 in ESR spectra (Figure 3.7 and Figure 3.12). Figure 3.13 shows that with addition of $Fe_2O_3$ content to $Cr_2O_5$ containing soda-lime-silicate glass, the signal intensities at g=5.2 and at g=2.1 increase and decrease, respectively. The rise of signal intensity at g=5.2 results from that with increasing amount of $Fe_2O_3$ content until 0.1 mol %, the signal at g=4.2 increase and overlap with signal at g=5.2. This overlapping causes rise of the signal at g=5.2. It is assumed that, the signal at g=5.2 ($Cr^{3+}$ ion located in glass network) is not affected from rise of anisotropy too much and $Cr^{3+}$ ions located in glass network have still powerful ESR signal. The signals of $Cr^{3+}$ ions at g=2.1 (comes from $Cr^{3+}$ clusters) decrease with increasing amount of $Fe_2O_3$ content as shown in Figure 3.13. It is assumed that, the signal of $Fe^{3+}$ at g=2.0 (come from $Fe^{3+}$ clusters) may overlap with the signal of $Cr^{3+}$ ions at g=2.1 and cancel them. Hence, the signal of $Cr^{3+}$ ions at g=2.1 decrease. Another explanation is that this signal loss results from increasing of anisotropy with addition of $Fe_2O_3$ content in glass [25].

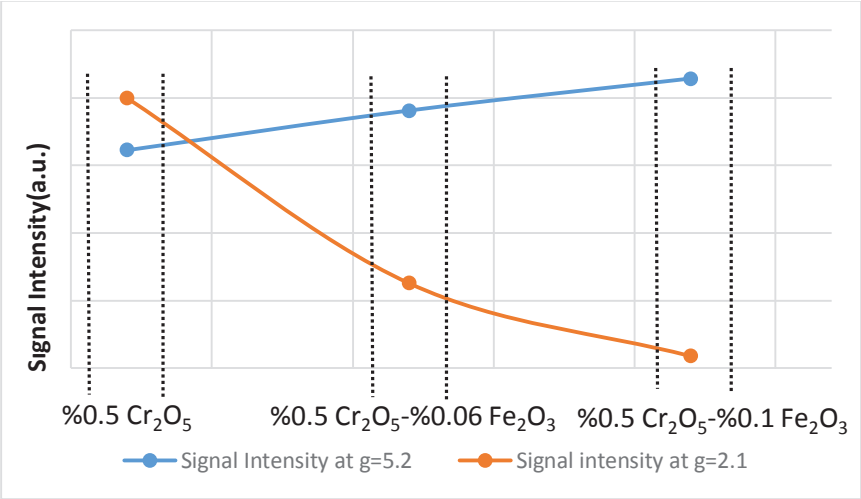


Figure 3.13. Signal intensity of $Cr^{3+}$ ions (in Figure 3.2 and Figure 3.12) at g=5.2 and g=2.1 vs. mol percentage of $Fe_2O_3$ and $Cr_2O_5$

### 3.1.3. $MnO_2$ Containing Soda-Lime-Silicate Glass

Figure 3.14, 3.15 and 3.16 show three levels of $MnO_2$ containing soda-lime-silicate glass samples with compositions; $25Na_2O$-$10CaO$-$65SiO_2$-$xMnO_2$ (x=0.1, 0.3, 0.5), $25Na_2O$-$10CaO$-$65SiO_2$-$0.05Fe_2O_3$-$xMnO_2$ (x=0.1, 0.3 and 0.5), $25Na_2O$-$10CaO$-$65SiO_2$-$0.3Fe_2O_3$-$xMnO_2$ (x=0.1, 0.3 and 0.5) after cooling process, respectively. $MnO_2$ gives purple color to glass (from Table 1.1) and the color intensity is directly proportional to $MnO_2$ concentration as shown in Figure 3.14 and 3.15. Color of each glass samples does not appear uniform due to depth of glass in crucible. When the depth of glass increases, the color intensity increases. Figure 3.16 shows that when the amount of $Fe_2O_3$ reaches at amount of $MnO_2$ levels in glass, color of glass starts to change from purple to green.

Figure 3.14. Crucible samples of [25$Na_2O$-10CaO-65$SiO_2$-x$MnO_2$ (x=0.1, 0.3 and 0.5 mol %)] after cooling process.

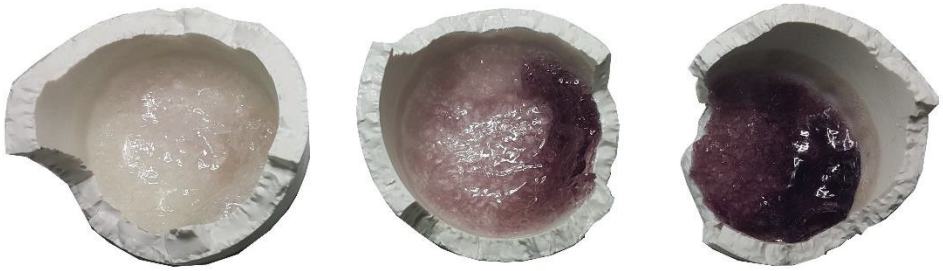

Figure 3.15. Crucible samples of [25$Na_2O$-10CaO-65$SiO_2$-0.05$Fe_2O_3$-x$MnO_2$ (x=0.1, 0.3 and 0.5 mol %)] after cooling process.

Figure 3.16. Crucible samples of [25$Na_2O$-10CaO-65$SiO_2$-0.3$Fe_2O_3$-x$MnO_2$ (x=0.1, 0.3 and 0.5 mol %)] after cooling process.

Figure 3.17 shows ESR spectrum of $MnO_2$ containing soda-lime-silicate glass with composition; 25$Na_2O$-10CaO-65$SiO_2$-0.5$MnO_2$. $Mn^{2+}$ has $d^5$ orbital and its total spin number is S=5/2. Hence, it splits into three Krames' doublets, ±5/2, ±3/2 and ±1/2. There are five ESR transitions are allowed between these Krames' doublets (-5/2→-3/2, -3/2→-1/2, -1/2→+1/2, +1/2→+3/2, +5/2→+3/2). However, -1/2→+1/2 transition is allowed for powder samples and other four transitions are not allowed due to the high anisotropy. $Mn^{2+}$ has also a nuclear spin I=5/2 that causes 6 hyperfine splittings (from 2I+1 formula). Figure 3.17 shows three significant characteristic values of g. The signal at g=5.0 is associated with strong rhombic distortion of octahedral symmetry of $Mn^{2+}$ ions in glass network [29]. The signal at g=4.2 is associated with $Fe^{3+}$ impurity [30] whose symmetry is rhombic distorted in glass network. The signal at g=2.0 consist of two types of signal which come from $Mn^{2+}$ clusters and hyperfine interaction of $Mn^{2+}$ ions. The first one is associated with elongation or tetragonal [31] distortion of octahedral symmetry of $Mn^{2+}$ ions that locate as clusters in glass and it is associated with $Mn^{2+}$-$Mn^{2+}$ spin interaction [32]. The second one is that sextet lines appear which arises from interaction between electron spin and nuclear spin in manganese ions, which is also called hyperfine interaction [29].

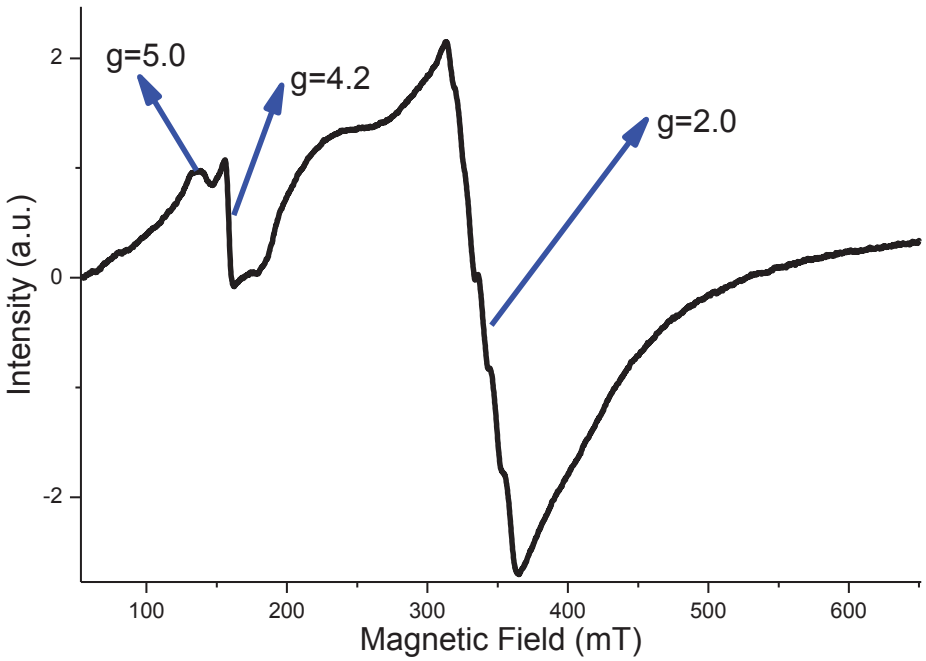


Figure 3.17. ESR spectrum of $MnO_2$ containing soda-lime-silicate glass [$25Na_2O$-10CaO-$65SiO_2$-$0.3MnO_2$ mol %]

Figure 3.18 shows the ESR spectra of 3 different levels (x=0.1, 0.3 and 0.5 mol %) of $MnO_2$ containing base compositions ($25Na_2O$-10CaO-$65SiO_2$), which were named as 7.1 to 7.3 at Table 2.2. Signal intensities at g=5.0 and g=2.0 increase with increasing amount of $MnO_2$. At g=2.0, the sextet lines (hyperfine splittings) vanish with increasing amount of $MnO_2$, which may be caused by signal overlapping of sextet lines. Another assumption is that the signal of $Mn^{2+}$-$Mn^{2+}$ spin interaction may suppress the sextet lines. Azzoni [33] claimed that these sextet lines disappear with high concentration of $MnO_2$ due to increasing of randomness in the position of $Mn^{2+}$ ions (which is also called anisotropy).

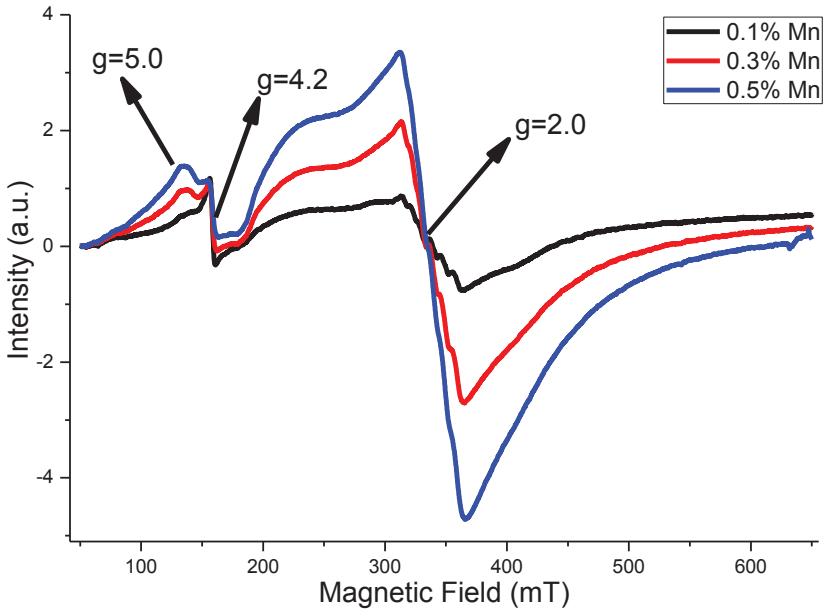


Figure 3.18. ESR spectra of $MnO_2$ containing glass samples [$25Na_2O$-$10CaO$-$65SiO_2$-$xMnO_2$(x=0.1, 0.3 and 0.5 mol %)]

The changes in the signal intensity as a function of amount of $MnO_2$ are different for g=2.0 and g=5.0. Figure 3.19 shows signal intensity of $Mn^{2+}$ ions versus mol percentage of $MnO_2$ in soda-lime-silicate glass from Figure 3.18. It is observed that increasing ratio of signal at g=2.0 is higher than increasing ratio of signal at g=5.0. As mentioned earlier, the signal at g=5.0 is associated with $Mn^{2+}$ ions in glass network and the signal at g=2.0 is associated with $Mn^{2+}$ ions located as cluster in glass. Hence, with increasing amount of $MnO_2$ content, amount of $Mn^{2+}$ ions in clusters increases more than the increase number of $Mn^{2+}$ ions in glass network. It is also supported with Figure 3.20 which shows location percentages of $Mn^{2+}$ ions in glass structure versus $MnO_2$ content in glass. It shows that percentage of $Mn^{2+}$ ions located as cluster in glass is much higher than $Mn^{2+}$ ions located in glass network and this difference increase with increasing content of $MnO_2$. It is assumed that the number of $Mn^{2+}$ ions in glass network starts to reach saturation level with increasing amount of $MnO_2$ content. That's why, $Mn^{2+}$ ions locate as clusters with higher percentage than $Mn^{2+}$ ions located in glass network.

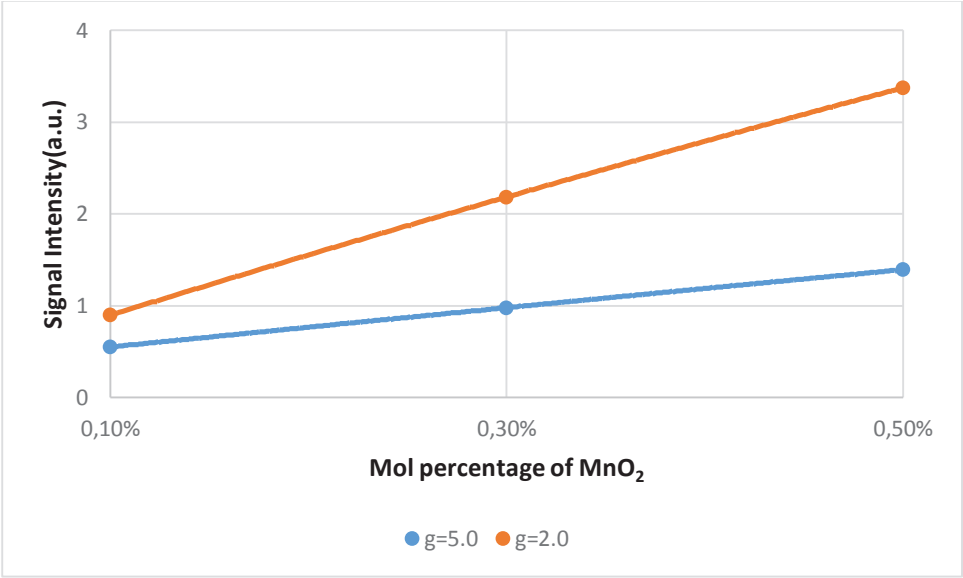


Figure 3.19. Signal intensity of $Mn^{2+}$ ions (from Figure 3.15) at g=5.0 and g=2.0 vs. mol percentage of $MnO_2$

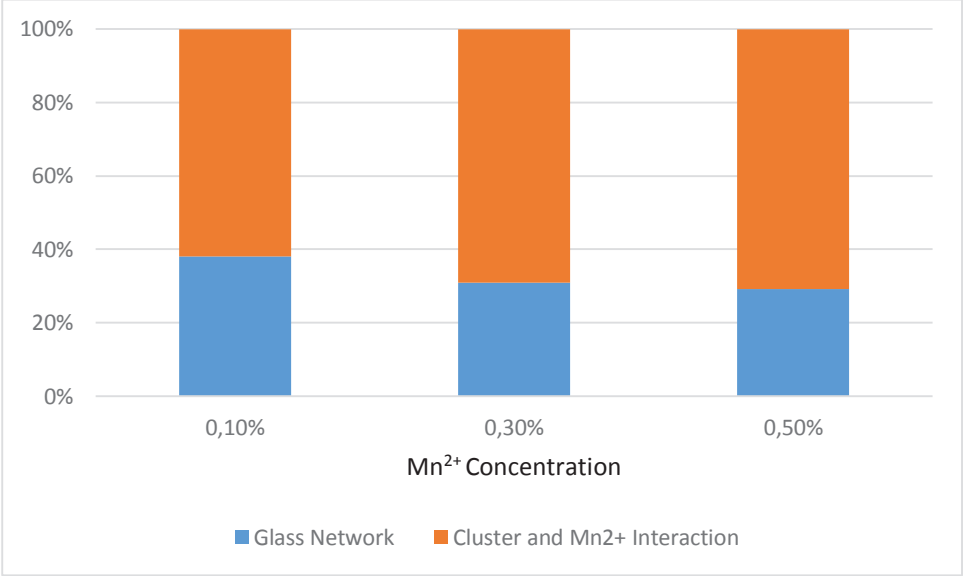


Figure 3.20. Location of $Mn^{2+}$ ions in glass vs. mol percentage of $MnO_2$

In order to analyze the ESR spectra of $Fe^{3+}$-$Mn^{2+}$ ion mixtures, two different $Fe_2O_3$ composition levels were used with 0.1, 0.2 and 0.3 $MnO_2$ mol % (compositions 8.1 to 8.6 at Table.2.2) as shown in Figure 3.21 and Figure 3.22.

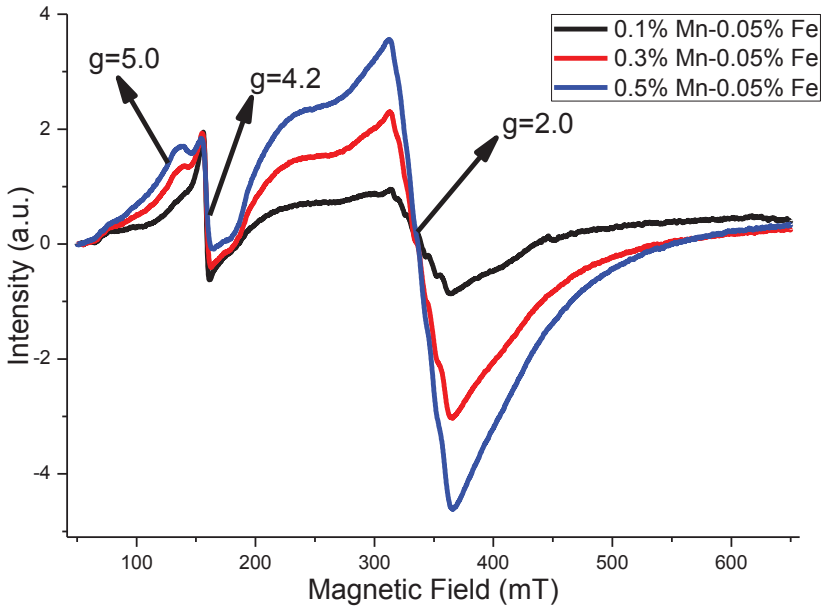


Figure 3.21. ESR spectra of $Fe_2O_3$ and $MnO_2$ containing glass samples [$25Na_2O$-$10CaO$-$65SiO_2$-$0.05Fe_2O_3$-$xMnO_2$ (x=0.1, 0.3 and 0.5 mol %)]

Figure 3.21 shows ESR spectra of glass samples after addition of 0.05 mol % $Fe_2O_3$ content to 3 different levels of $MnO_2$ containing base compositions ($25Na_2O$-$10CaO$-$65SiO_2$), which were named as 8.1 to 8.3 at Table 2.2. Signal intensities at g=5.0 and g=2.0 increase with increasing $MnO_2$ content. The sextet lines at g=2.0 also start to vanish. These signals behaviors are same with the only $MnO_2$ containing soda-lime-silicate glass samples (Figure 3.18). The signal at g=4.2 is associated with the rhombic distortion of tetrahedral or octahedral coordination of $C_{2v}$ symmetry of $Fe^{3+}$ ions which locate in glass network [16]. This signal has higher intensity than the intensity of signal at g=4.2 in Figure 3.18 (just $MnO_2$ containing soda-lime-silicate glass samples) with addition of %0.05 $Fe_2O_3$ content. However, this signal rise is not proportional to or equal with summation of signal intensities of $Fe^{3+}$ and $Mn^{2+}$ at g=4.2. It is assumed that this nonequivalence results from signal overlapping or signal loss due to anisotropy.

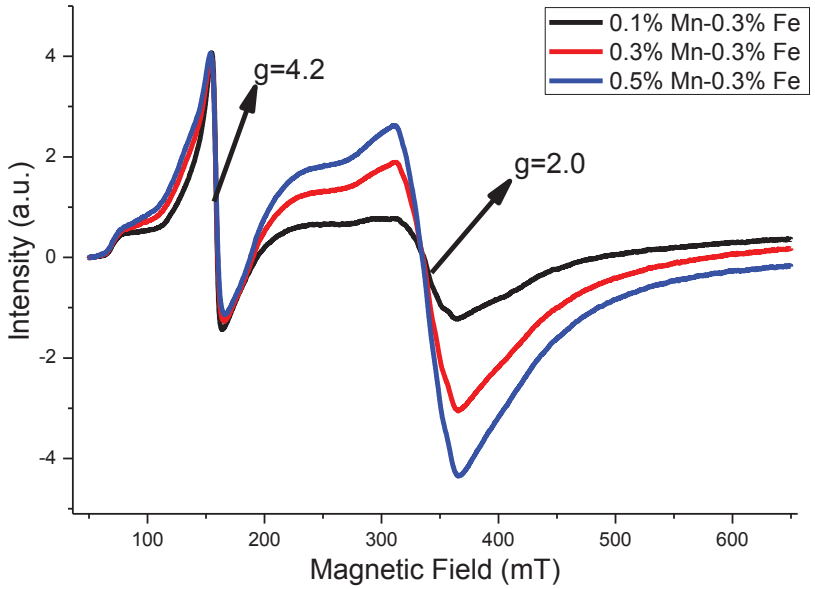


Figure 3.22. ESR spectra of $Fe_2O_3$ and $MnO_2$ containing glass samples [$25Na_2O$-$10CaO$-$65SiO_2$-$0.3Fe_2O_3$-$xMnO_2$ (x=0.1, 0.3 and 0.5 mol %)]

Figure 3.22 shows ESR spectra of glass samples after addition of 0.3 mol % $Fe_2O_3$ content to 3 different levels of $MnO_2$ containing base compositions ($25Na_2O$-$10CaO$-$65SiO_2$), which were named as 8.4 to 8.6 at Table 2.2. Signal intensities at g=5.0 and g=2.0 increase with increasing amount of $Cr_2O_5$. The signal at g=5.0 (signal of $Mn^{2+}$ ions) cannot be seen well in comparison to other two ESR spectra (Figure 3.19 and Figure 3.20) with addition of 0.3 mol % level of $Fe_2O_3$ content to MnO containing soda-lime-silicate glass. It is assumed that $Fe^{3+}$ signal at g=4.2 may block signal of $Mn^{2+}$ at g=5 or the signal of $Mn^{2+}$ ions cannot seen due to anisotropy. At g=2, hyperfine splittings cannot be observed accurately, which is caused by 0.3 mol % concentration of $Fe_2O_3$. Increasing amount of $Fe^{3+}$ content in glass causes anisotropy in glass or rise of randomness in position of $Mn^{2+}$ ions in glass. As mentioned by Azzoni [33], these randomness may cause disappearance of sextet lines (hyperfine splittings) at g=2.0.

### 3.1.4. CuO Containing Soda-Lime-Silicate Glass

Figure 3.23, 3.24 and 3.25 show three levels of CuO containing soda-lime-silicate glass samples with these compositions (samples 5.1 to 6.6 from Table 2.2) ; $25Na_2O$-$10CaO$-$65SiO_2$-$xCr_2O_5$ (x=0.1, 0.3 and 0.5 mol %), $25Na_2O$-$10CaO$-$65SiO_2$-$0.05Fe_2O_3$-$xMnO_2$ (x=0.1, 0.3 and 0.5 mol %) and $25Na_2O$-$10CaO$-$65SiO_2$-$0.3Fe_2O_3$-$xMnO_2$ (x=0.1,

0.3 and 0.5 mol %) after cooling process. CuO gives light blue color to glass (from Table 1.1) and color intensity is directly proportional to CuO concentrations. Figure 3.25 shows that when amount of $Fe_2O_3$ reaches at amount of CuO levels in glass, color of glass starts to change from light blue to green color.

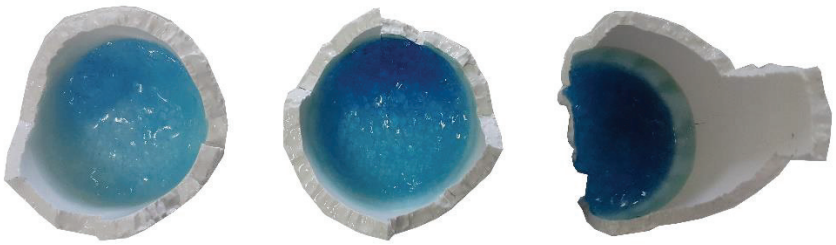

Figure 3.23. Crucible samples of [$25Na_2O$-10CaO-$65SiO_2$-xCuO(x=0.1, 0.3 and 0.5 mol %)] after cooling process.

Figure 3.24. Crucible samples of [$25Na_2O$-10CaO-$65SiO_2$-$0.05Fe_2O_3$-x$MnO_2$(x=0.1, 0.3 and 0.5 mol %)] after cooling process.

Figure 3.25. Crucible samples of [25$Na_2O$-10CaO-65$SiO_2$-0.3$Fe_2O_3$-x$MnO_2$ (x=0.1, 0.3 and 0.5 mol %)] after cooling process.

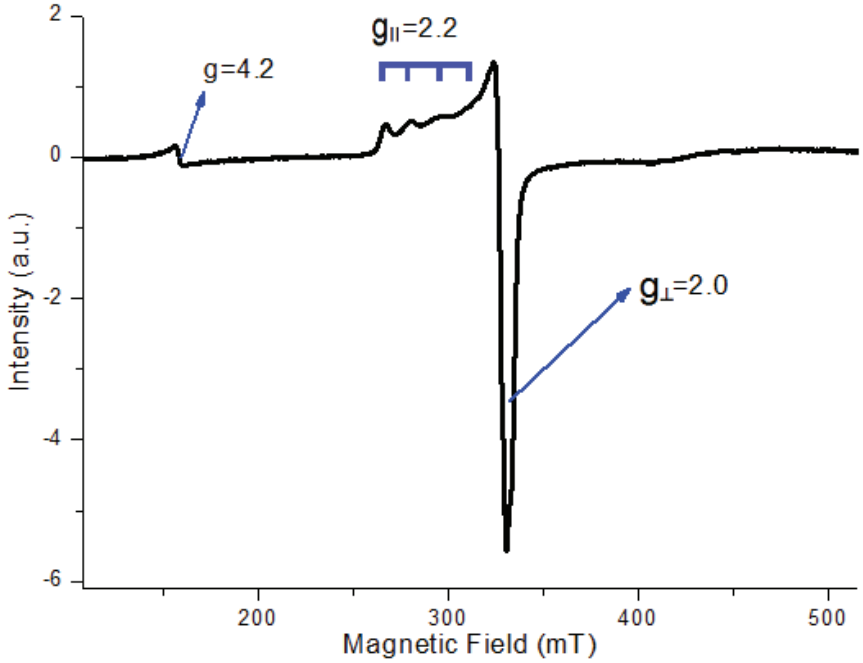


Figure 3.26. ESR spectrum of [25$Na_2O$-10CaO-65$SiO_2$-0.5CuO mol %]

Figure 3.26 shows ESR spectrum of CuO containing soda-lime-silicate glass with composition; 25$Na_2O$-10CaO-65$SiO_2$-0.5CuO. $Cu^{2+}$ has $d^9$ orbital and its spin number is S=1/2. $Cu^{2+}$ ions located octahedral symmetry in glass. If octahedral symmetry of isolated (located in glass network) $Cu^{2+}$ ions elongate (or distort tetragonally) parallel to z-axis, it is represented as $g_{\shortparallel}$ and its value around g=2.2. If octahedral symmetry of isolated $Cu^{2+}$ ions elongate (or distort tetragonally) perpendicular to z-axis, it is represented as $g_{\perp}$ and

its value around g=2.0 as shown in Figure 3.26 [34]. $Cu^{2+}$ ion has a nuclear spin (I=3/2) that causes 4 hyperfine splittings (from 2I+1 formula). The signal at g=4.2 is associated with $Fe^{3+}$ impurity whose symmetry is rhombic distorted in glass network [25].

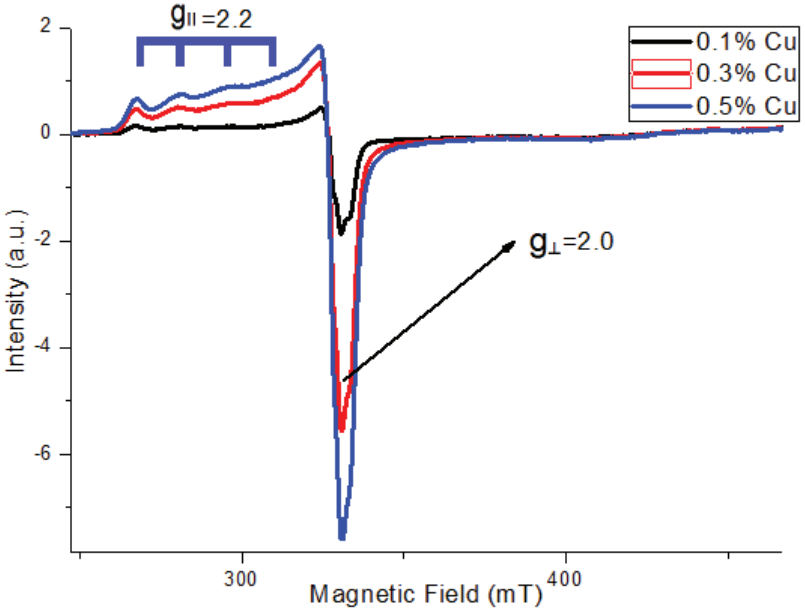


Figure 3.27. ESR spectra of CuO containing glass samples [25$Na_2O$-10CaO-65$SiO_2$-xCuO (x=0.1, 0.3 and 0.5 mol %)]

Figure 3.27 shows ESR spectra of 3 different levels of CuO containing base compositions (25$Na_2O$-10CaO-65$SiO_2$), which were named as 5.1 to 5.3 at Table 2.2. Signal intensities at g=2.2 and g=2.0 increase with increasing amount of CuO. The signal at g=4.2 is not shown in spectra because it is associated with impurity of $Fe^{3+}$ ions and it does not show any difference with respect to changing amount of CuO content in soda-lime-silicate glass. Four parallel hyperfine splittings ($g_{\parallel}$) would be expected at $g_{\parallel}$ =2.2, and these splittings resolved better with increasing amount of CuO content. Four hyperfine splittings would be expected at $g_{\perp}$=2.0 but they are not resolved very well due to the anisotropy. However, with decreasing amount of CuO, these splittings start to appear as shown in sample 0.1 mol % CuO containing soda-lime-silicate glass in Figure 3.27 [25].

In order to observe $Fe^{3+}$-$Cu^{2+}$ interactions, two different $Fe_2O_3$ compositions were used with 0.1, 0.2 and 0.3 CuO mol % (compositions 6.1 to 6.6 at Table.2.2) as shown in Figure 3.28 and Figure 3.29.

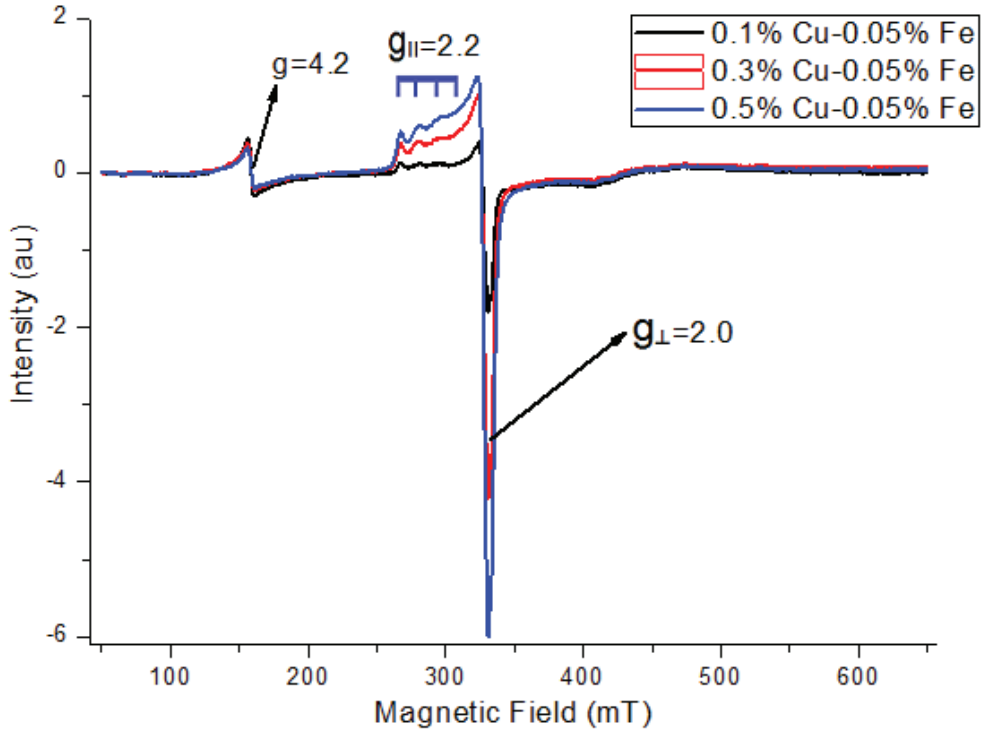


Figure 3.28. ESR spectra of $Fe_2O_3$ and CuO containing glass samples [$25Na_2O$-10CaO-$65SiO_2$-$0.05Fe_2O_3$-xCuO (x=0.1, 0.3 and 0.5 mol %)]

Figure 3.28 shows ESR spectra of glass samples after addition of 0.05 mol % $Fe_2O_3$ addition to 3 levels of CuO with these compositions; $25Na_2O$-10CaO-$65SiO_2$-$0.05Fe_2O_3$-xCuO (x=0.1, 0.3 and 0.5 mol %). The signal intensity at g=4.2 which is associated with rhombic distorted octahedral symmetry of $Fe^{3+}$ ions in glass network increase with addition of 0.05 mol % $Fe_2O_3$ content in comparison to Figure 3.26. Signal at $g_{\perp}$=2.0 which is associated with $Fe^{3+}$ locating as cluster in glass structure is blocked by $Cu^{2+}$ signal at $g_{\perp}$=2.0.

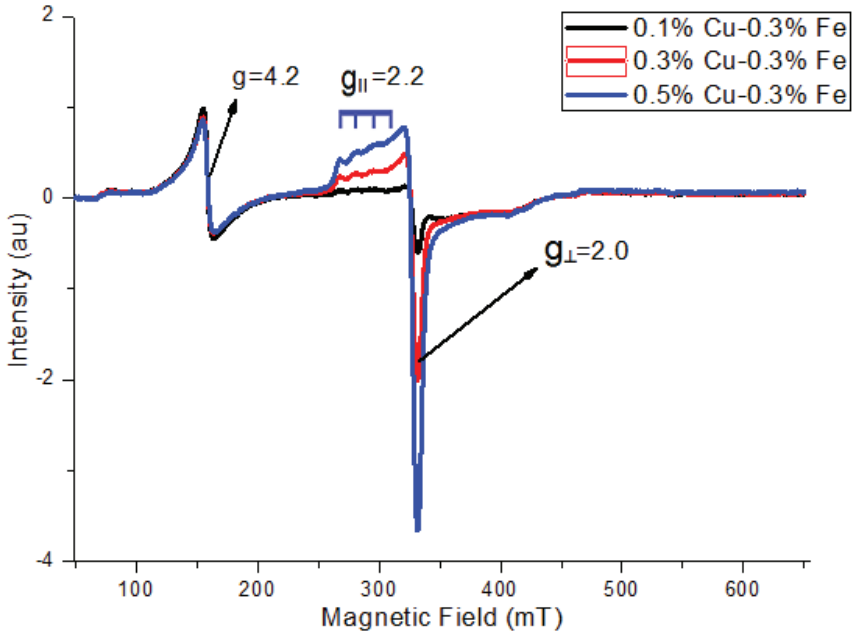


Figure 3.29. ESR spectra of $Fe_2O_3$ and CuO containing glass samples [$25Na_2O$-10CaO-$65SiO_2$-$0.3Fe_2O_3$-xCuO x=0.1, 0.3 and 0.5 mol %)]

Figure 3.29 shows ESR spectra of glass samples after addition of 0.3 mol % $Fe_2O_3$ addition to 3 levels of CuO with these compositions; $25Na_2O$-10CaO-$65SiO_2$-$0.3Fe_2O_3$-xCuO (x=0.1, 0.3 and 0.5 mol %). The signal intensity at g=4.2 which is associated with rhombic distorted octahedral symmetry of $Fe^{3+}$ in glass network increases with addition of 0.3 mol % $Fe_2O_3$ content in comparison to Figure 3.26 and Figure 3.28. Signal at g=2.0 which is associated with $Fe^{3+}$ locating as cluster in glass structure is blocked by $Cu^{2+}$ signal at $g_{\perp}$=2.0.

### 3.1.5. General Overview

In order to observe effects of $Cr^{3+}$, $Mn^{2+}$ and $Cu^{2+}$ ions on $Fe^{3+}$ ions, ESR spectra of pure $Cr_2O_5$, $MnO_2$ and CuO containing soda-lime-silicate glasses (from Figure 3.7, Figure 3.18 and Figure 3.27, respectively) is subtracted from ESR spectra of $Cr_2O_5$-$Fe_2O_3$, $MnO_2$-$Fe_2O_3$ and CuO-$Fe_2O_3$ (from Figure 3.10-3.11, Figure 3.21-3.22 and Figure 3.28-3.29, respectively) containing soda-lime-silicate glasses, respectively. As shown in Figure 3.30 to Figure 3.35, when transition metals ($Cr^{3+}$, $Mn^{2+}$ and $Cu^{2+}$) were added to $Fe_2O_3$ containing soda-lime-silicate glasses, the signal of $Fe^{3+}$ ions at g=4.2 (located in glass network) decreases. This signal loss may result from replacing of $Cr^{3+}$, $Mn^{2+}$ or $Cu^{2+}$

ions with octahedral or tetrahedral symmetry of $Fe^{3+}$ ions which are located in glass network or these transition metals may reduce $Fe^{3+}$ ions into diamagnetic $Fe^{2+}$ ions In another assumption is,addition of transition metals ($Cr^{3+}$, $Mn^{2+}$ and $Cu^{2+}$) causes high randomness of $Fe^{3+}$ (or anisotropy) in glass. Therefore the signal of $Fe^{3+}$ ions located in glass network decreases [25].

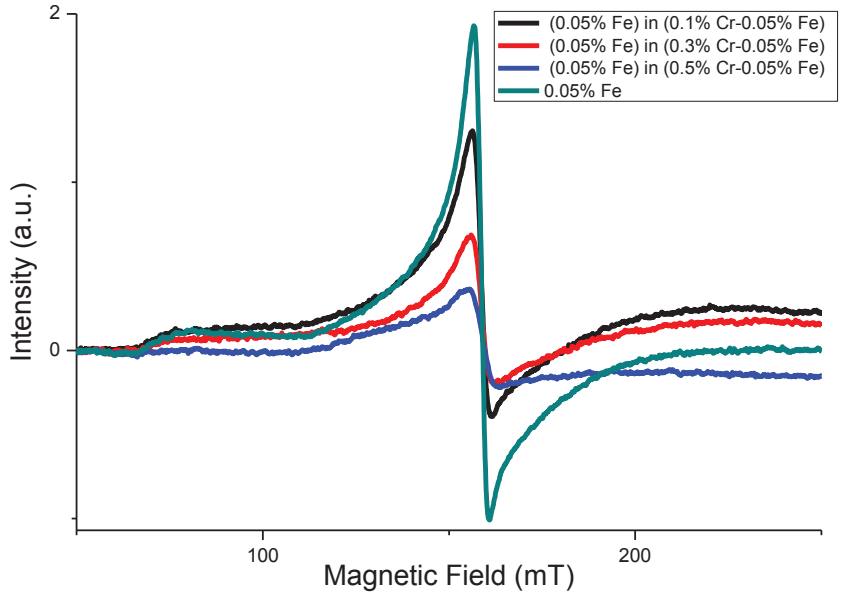


Figure 3.30. ESR spectra of $Fe^{3+}$ ion at g=4.2 in glass samples; [$25Na_2O$-$10CaO$-$65SiO_2$-$0{,}05Fe_2O_3$-$xCr_2O_5$ (x=0.1, 0.3 and 0.5 mol %)]

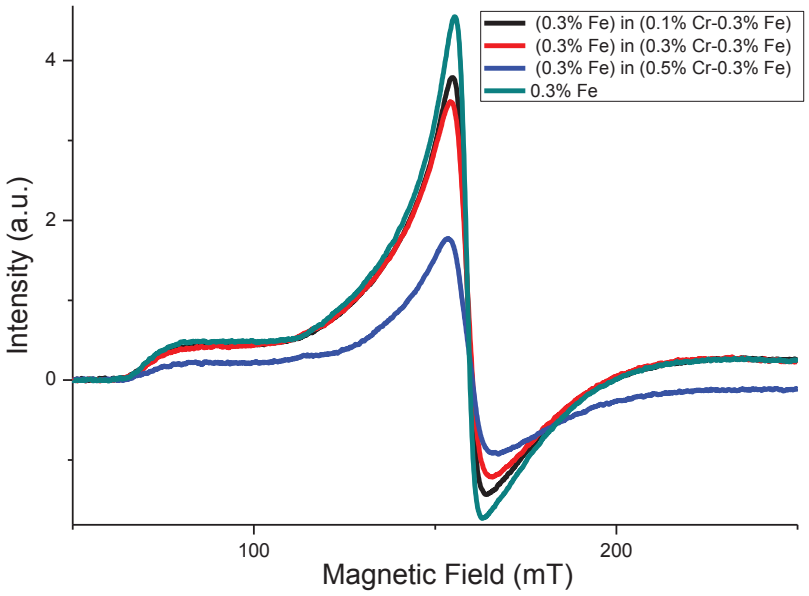


Figure 3.31. ESR spectra of $Fe^{3+}$ ion at g=4.2 in glass samples; [$25Na_2O$-$10CaO$-$65SiO_2$-$0{,}3Fe_2O_3$-$xCr_2O_5$ (x=0.1, 0.3 and 0.5 mol %)]

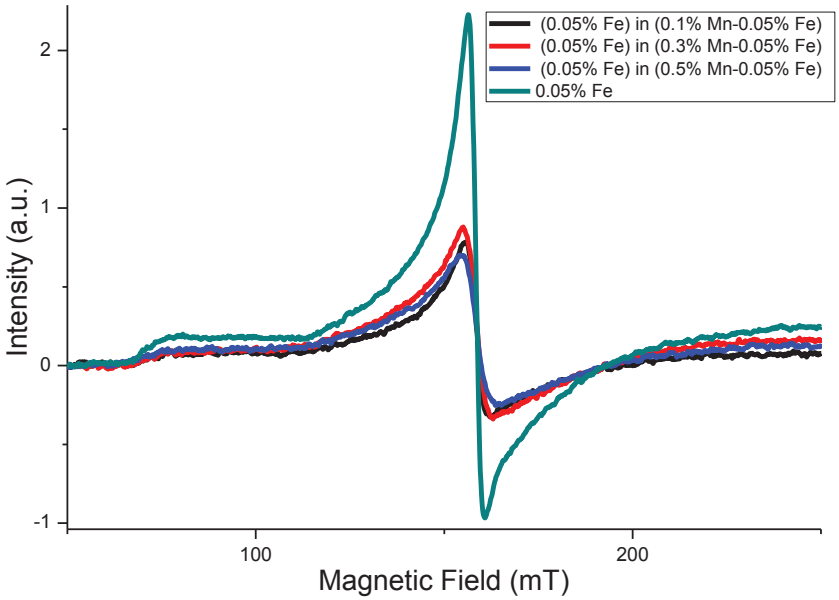


Figure 3.32. ESR spectra of $Fe^{3+}$ ion at g=4.2 in glass samples; [$25Na_2O$-$10CaO$-$65SiO_2$-$0{,}05Fe_2O_3$-$xMnO_2$ x=0.1, 0.3 and 0.5 mol %)]

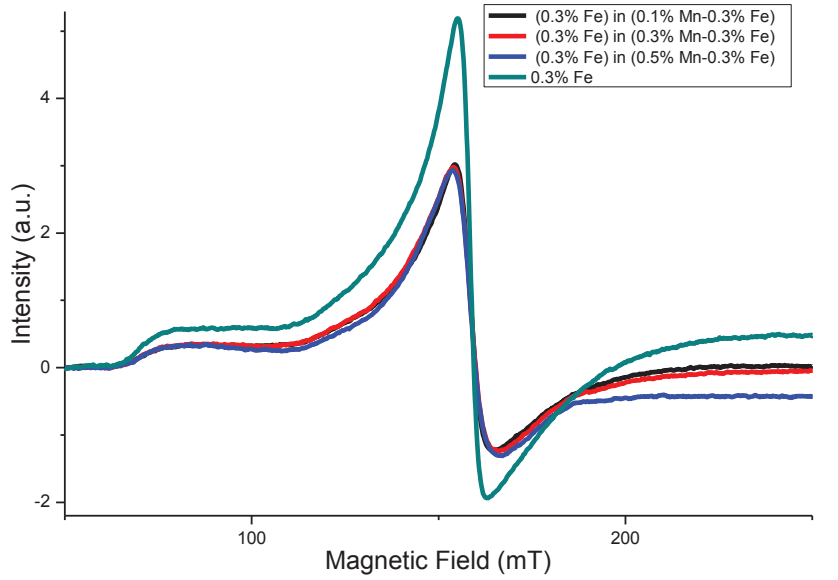


Figure 3.33. ESR spectra of $Fe^{3+}$ ion at g=4.2 in glass samples; [$25Na_2O$-$10CaO$-$65SiO_2$-$0{,}3Fe_2O_3$-$xMnO_2$ (x=0.1, 0.3 and 0.5 mol %)]

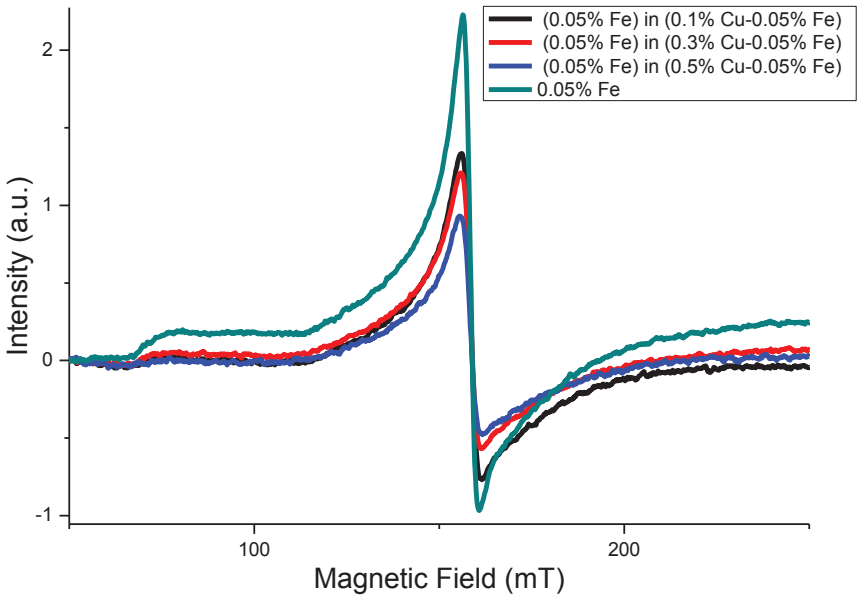


Figure 3.34. ESR spectra of $Fe^{3+}$ ion at g=4.2 in glass samples; [25$Na_2O$-10CaO-65$SiO_2$-0,05$Fe_2O_3$-xCuO (x=0.1, 0.3 and 0.5 mol %)]

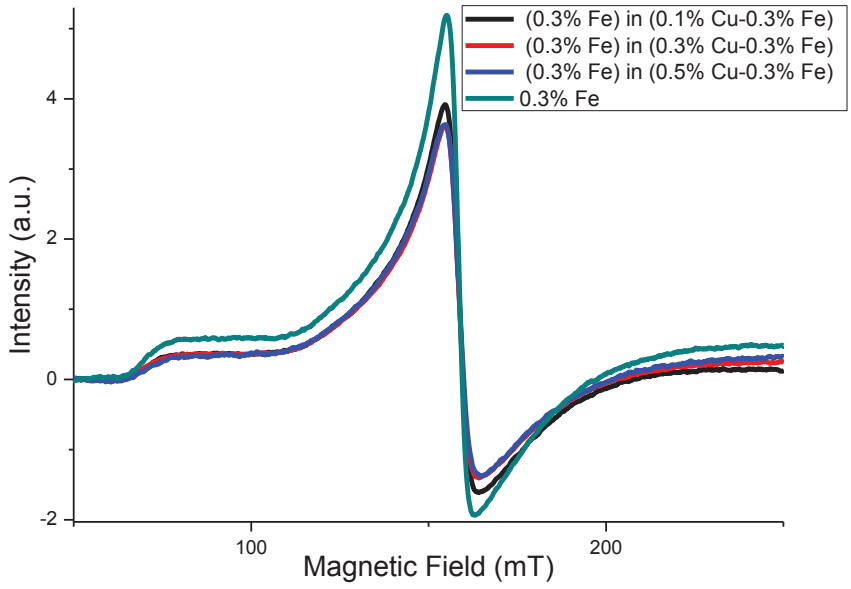


Figure 3.35. ESR spectra of $Fe^{3+}$ ion at g=4.2 in glass samples; [25$Na_2O$-10CaO-65$SiO_2$-0,3$Fe_2O_3$-xCuO (x=0.1, 0.3 and 0.5 mol %)]

## 3.2. XPS Measurements

In order to differentiate $Fe^{3+}$ and $Fe^{2+}$ ions quantitatively in soda-lime-silicate glass, X-ray photoelectron spectroscopy (XPS) was used. 0.3%, 0.5% and 1.0% mol $Fe_2O_3$ containing soda-lime-silicate glasses were measured and 2p orbitals of iron ions were scanned by XPS spectrometer. However, X-ray photoelectron spectrometer could not differentiate iron ions under level of 1.0% mol $Fe_2O_3$ as shown in Figure 3.36 and Figure 3.38. Even 1.0% mol $Fe_2O_3$ containing soda-lime-silicate glass sample cannot be differentiated precisely by XPS as shown in Figure 3.38. These results showed that X-ray photoelectron spectrometer is not as precise as ESR spectrometer at low levels (range of 0.0%-1.0% mol).

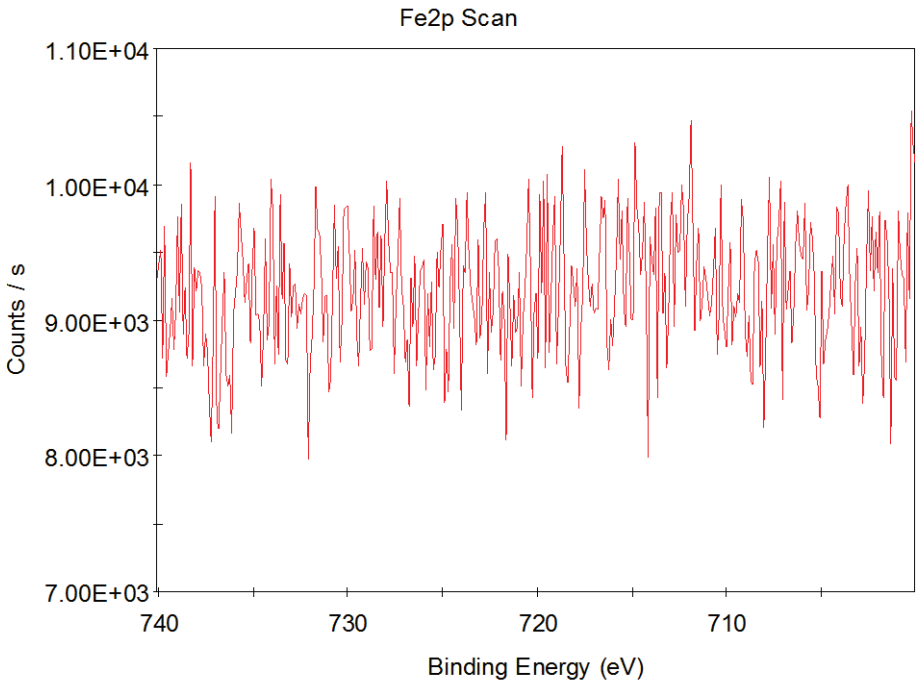


Figure 3.36. XPS spectra of [25$Na_2O$-10CaO-65$SiO_2$-0.3$Fe_2O_3$ mol %].

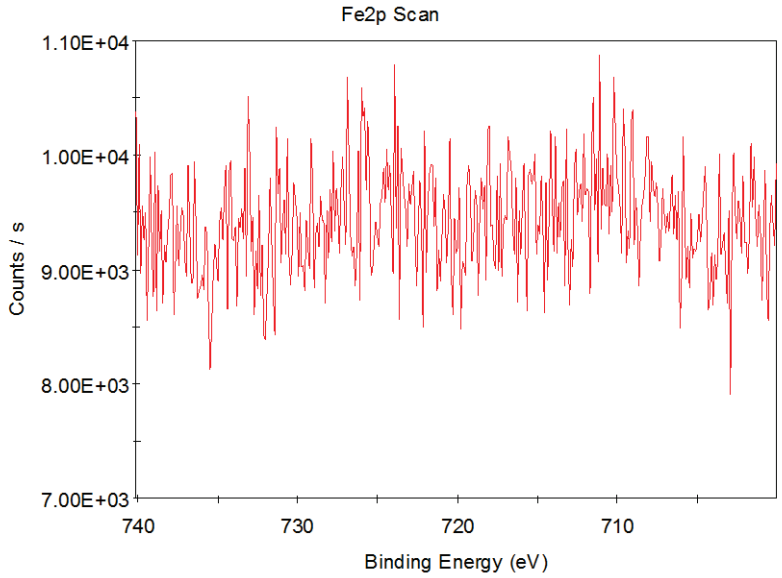


Figure 3.37. XPS spectra of [25$Na_2O$-10CaO-65$SiO_2$-0.5$Fe_2O_3$ mol %]

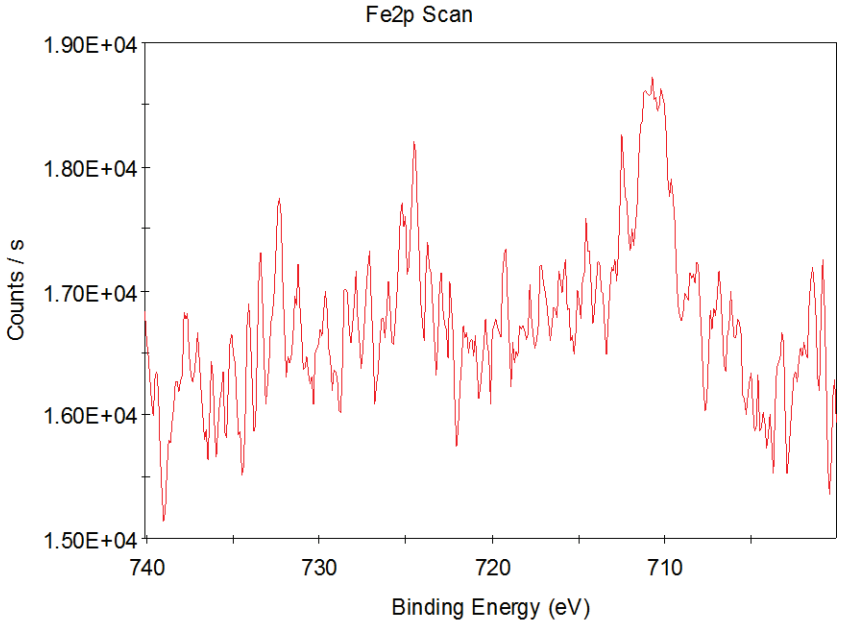


Figure 3.38. XPS spectra of [25$Na_2O$-10CaO-65$SiO_2$-1.0$Fe_2O_3$ mol %]

# CHAPTER 4

# SUMMARY AND CONCLUSIONS

This study showed the behavior and interaction of paramagnetic 3d transition metal ions ($Fe^{3+}$, $Cr^{3+}$, $Mn^{2+}$ and $Cu^{2+}$) at low addition levels by using ESR spectroscopy in soda-lime-silicate based glasses. The results obtained from the ESR measurements of $Fe_2O_3$ containing glasses showed signals at g=4.2 and g=2.0, in agreement with the literature. These signals are associated with $Fe^{3+}$ ions located in glass network for g=4.2, and with $Fe^{3+}$ ions located as a cluster as well as $Fe^{3+}$- $Fe^{3+}$ interaction for g=2.0 [14]. The results further showed the intensities of the signals at these two g values to be effected by the concentration of $Fe_2O_3$ in the glass composition. ESR technique can reveal the types of $Fe^{3+}$ ions in glass even at low addition levels (below 1.0 mol % $Fe_2O_3$). When the concentration level of $Fe_2O_3$ reaches 1.0 mol % in glass, percentage of $Fe^{3+}$ ions that locate as cluster increases more than the percentage of $Fe^{3+}$ ions in glass network. It is assumed that Fe ions in glass network starts to reach saturation level with addition of $Fe_2O_3$. XPS analysis was done in order to further support the quantification of the ESR data of the $Fe_2O_3$ in the glass composition. However, XPS was ineffective at low addition levels (below 1.0 mol % $Fe_2O_3$). While XPS was found to be inadequate in quantifying the paramagnetic $Fe^{3+}$ ions at low addition levels, the results of ESR spectroscopy were shown to provide trends in the relative structural formation of $Fe^{3+}$ ions either as part of the glass network or as clusters outside of the network structure.

Furthermore, when other transition metals ($Cr^{3+}$, $Mn^{2+}$ or $Cu^{2+}$) were added to $Fe_2O_3$ containing glass compositions, the signal at g=4.2 for $Fe^{3+}$ decreases. This result is assumed to be either replacement of $Cr^{3+}$, $Mn^{2+}$ or $Cu^{2+}$ ions with $Fe^{3+}$ ions which are located in glass network or these transition metals may reduce $Fe^{3+}$ ions into diamagnetic $Fe^{2+}$ ions. Another assumption is that with addition of these transition metals ($Cr^{3+}$, $Mn^{2+}$ or $Cu^{2+}$), ESR signal intensity of $Fe^{3+}$ ions decrease due to the anisotropy increases [22, 24]. The ESR spectra of $Cr_2O_5$, MnO, and CuO containing glasses have been analyzed as follows:

- ESR measurement of $Cr_2O_5$ containing glass showed signals at g=5.2, g=2.1 and g=2.0, in line with the literature. These signals have been linked to $Cr^{3+}$ ion located

in glass network for g=5.2, and to $Cr^{3+}$ and $Cr^{5+}$ located as cluster and transition metal-metal interaction for signals at g=2.1 and g=2.0, respectively [22, 24].

- ESR measurement of $MnO_2$ doped glass shows signals at g=5.0 and g = 2.0, which are associated with $Mn^{2+}$ ion located in glass network and signal at g=2.0 which is also associated with $Mn^{2+}$ ion located as cluster and $Mn^{2+}$- $Mn^{2+}$ interaction. At g=2.0 there are also sextet lines appear which is associated with hyperfine interaction of $Mn^{2+}$ ions [29].
- ESR measurement of CuO doped glass shows signals at $g_{II}$=2.2 and $g_{\perp}$=2.0. The signal at $g_{\perp}$=2.0 which has been associated with octahedral sites of $Cu^{2+}$ ions elongated perpendicular to z-axis in glass network and signal at $g_{II}$=2.2 which has been linked with octahedral sites of $Cu^{2+}$ ions elongated parallel to z-axis. At $g_{II}$=2.2, quartet lines appear, which is associated with hyperfine interaction of $Cu^{2+}$ ions [34].

# REFERENCES


1. Varshneya, A. K., *Fundamentals of Inorganic Glasses*. 1 ed.; 1994.

2. Park, J. B., *Bioceramics : properties, characterizations, and applications*. Springer: New York, 2008; p xii, 359 p.

3. Shelby, J. E., *Introduction to Glass Science and Technology*. 2 ed.; 2005.

4. Zavoisky, E., Spin-magnetic resonance in paramagnetics. *Fizicheskiĭ Zhurnal* **1945,** *9*.

5. Odom, B.; Hanneke, D.; D'Urso, B.; Gabrielse, G., New measurement of the electron magnetic moment using a one-electron quantum cyclotron. *Phys Rev Lett* **2006,** *97* (3).

6. Abraham, A.; Bleaney, B., *Electron Paramagnetic Resonance of Transition Ions*. 1986.

7. Wertz, J. E.; Bolton, J. R., *Electron spin resonance: Elementary theory and practical applications*. 1972.

8. Cornu, L.; Duttine, M.; Gaudon, M.; Jubera, V., Luminescence switch of Mn-Doped ZnAl2O4 powder with temperature. *J Mater Chem C* **2014,** *2* (44), 9512-9522.

9. Merzbacher, E., *Quantum Mechanics* 3ed.; John Wiley: New York, 1998.

10. Atherton, N. M., *Principles of electron spin resonance*. Ellis Horwood PTR Prentice Hall, 1993.

11. Kapteijn, F.; RodriguezMirasol, J.; Moulijn, J. A., Heterogeneous catalytic decomposition of nitrous oxide. *Appl Catal B-Environ* **1996,** *9* (1-4), 25-64.

12. R. Resnick, R. E., John Wiley & Sons,, *Quantum Physics of Atoms, Molecules, Solids, Nuclei and Particles* 2ed.; 1985.

13. Weil, J. A.; Wertz; J.E. and Bolton, J. R.; McGraw-Hill; Wiley, J., *Electron Paramagnetic Resonance: Elementary Theory and Practical Applications* 2ed.; 1994.

14. Fu, C. M.; Korchak, V. N.; Hall, W. K., Decomposition of Nitrous-Oxide on Fey Zeolite. *J Catal* **1981,** *68* (1), 166-171.

15. Perez-Ramirez, J.; Kapteijn, F.; Mul, G.; Moulijn, J. A., NO-assisted N2O decomposition over Fe-based catalysts: Effects of gas-phase composition and catalyst constitution. *J Catal* **2002,** *208* (1), 211-223.

16. Ruangthaweep, Y.; Kittiauchawal, T.; Kaewkhao, J.; Thamaphat, K.; Limsuwan, P., The Spectroscopic Analysis of Iron-Doped Soda-Lime-Silica Glass by Spectrophotometer and ESR Spectrometer. *Adv Mater Res-Switz* **2010,** *93-94*, 312-+.

17. Russel, C., Iron Oxide-Doped Alkali Lime Silica Glasses .1. Epr Investigations. *Glastech Ber-Glass* **1993,** *66* (3), 68-75.

18. Russel, C., EPR and voltammetric studies of iron-containing mixed alkali glasses with the basic composition xNa(2)O center dot(16-x)K2O center dot 10CaO center dot 74SiO(2). *Glastech Ber-Glass* **1997,** *70* (1), 17-22.

19. Srisittipokakun, N.; KedKaew, C.; Kaewkhao, J.; Kittiauchawal, T.; Thamaphat, K.; Limsuwan, P., Electron Spin Resonance (ESR) and Optical Absorption Spectra of a Manganese Doped Soda-Lime-Silicate Glass System. *Kasetsart J. (Nat. Sci.)* **2009,** *43*, 360 - 364.

20. Iwamoto, N.; Makino, Y., State of the Chromium Ion in Soda Silicate-Glasses under Various Oxygen Pressures. *J Non-Cryst Solids* **1980,** *41* (2), 257-266.

21. DAcapito, F.; Colonna, S.; Mobilio, S.; Gonella, F.; Cattaruzza, E.; Mazzoldi, P., Local atomic environment of Cu ions in ion-exchanged silicate glass waveguides: An x-ray absorption spectroscopy study. *Appl Phys Lett* **1997,** *71* (18), 2611-2613.

22. Kesavulu, C. R.; Chakradhar, R. P. S.; Jayasankar, C. K.; Rao, J. L., EPR, optical, photoluminescence studies of Cr3+ ions in Li2O-Cs2O-B2O3 glasses - An evidence of mixed alkali effect. *J Mol Struct* **2010,** *975* (1-3), 93-99.

23. Rao, J. L.; Sreedhar, B.; Reddy, M. R.; Lakshman, S. V. J., Electron-Spin Resonance and Optical-Absorption Spectra of Cr-3+ and Cu-2+ Ions in K2so4-Znso4 Glasses. *J Non-Cryst Solids* **1989,** *111* (2-3), 228-237.

24. Kesavulu, C. R.; Chakradhar, R. P. S.; Muralidhara, R. S.; Rao, J. L.; Anavekar, R. V., EPR, optical absorption and photoluminescence properties of Cr3+ ions in lithium borophosphate glasses. *J Alloy Compd* **2010,** *496* (1-2), 75-80.

25. Drzewiecki, A.; Padlyak, B.; Adamiv, V.; Burak, Y.; Teslyuk, I., EPR spectroscopy of Cu2+ and Mn2+ in borate glasses. *Nukleonika* **2013,** *58* (3), 379-385.

26. Prakash, P. G.; Rao, J. L., Cu2+ ions in sodium fluoride-sodium borate glasses studied by EPR and optical absorption techniques. *J Mater Sci* **2004,** *39* (1), 193-200.

27. Slappendel, S.; Veldink, G. A.; Vliegenthart, J. F. G.; Aasa, R.; Malmstrom, B. G., A Quantitative Optical and Electron-Paramagnetic-Res Study on the Interaction between Soybean Lipoxygenase-1 and 13-L-Hydroperoxylinoleic Acid. *Biochim Biophys Acta* **1983,** *747* (1-2), 32-36.

28. Fukamachi, C. R. B.; Wypych, F.; Mangrich, A. S., Use of Fe3+ ion probe to study the stability of urea-intercalated kaolinite by electron paramagnetic resonance. *J Colloid Interf Sci* **2007,** *313* (2), 537-541.

29. Stefan, R.; Simon, S., EPR of Mn2+ and Fe3+ ions doped in bismuth-borate glasses. *Mod Phys Lett B* **2001,** *15* (3), 111-117.

30. Baesso, M. L.; Mansanares, A. M.; Dasilva, E. C.; Vargas, H.; Miranda, L. C. M., Phase-Resolved Photoacoustic-Spectroscopy and Epr Investigation of Mno2-Doped and Coo-Doped Soda-Lime Glasses. *Phys Rev B* **1989,** *40* (3), 1880-1884.

31. Janes, R. M., E. A. , *Metal-ligand bonding*. 2004.

32. Terczynska-Madej, A.; Cholewa-Kowalska, K.; Laczka, M., The effect of silicate network modifiers on colour and electron spectra of transition metal ions. *Opt Mater* **2010,** *32* (11), 1456-1462.

33. Azzoni, C. B.; Di Martino, D.; Chiavari, C.; Martini, M.; Sibilia, E.; Vandini, M., Electron paramagnetic resonance of mosaic glasses from the Mediterranean area. *Archaeometry* **2002,** *44*, 543-554.

34. Purnima, M.; Edukondalu, A.; Kumar, K. S.; Rahman, S., EPR and Optical Absorption Studies of Cu2+ in Boro-Arsenate Glasses. *Mater Res-Ibero-Am J* **2017,** *20* (1), 46-52.